

# Structural and metal-insulator transitions in rhenium based double perovskites via orbital ordering

Alex Taekyung Lee and Chris A. Marianetti  
*Department of Applied Physics and Applied Mathematics,  
Columbia University, New York, New York 10027, USA*  
(Dated: August 28, 2017)

Re-based double perovskites (DPs) exhibit a complex interplay of structural and metal-insulator transitions. Here we systematically study the ground state electronic and structural properties for a family of Re-based DPs  $A_2B\text{ReO}_6$  ( $A=\text{Sr}, \text{Ca}$  and  $B=\text{Cr}, \text{Fe}$ ), which are related by a common low energy Hamiltonian, using density functional theory +  $U$  calculations. We show that the on-site interaction  $U$  of Re induces orbital ordering (denoted COO), with each Re site having an occupied  $d_{xy}$  orbital and a C-type alternation among  $d_{xz}/d_{yz}$ , resulting in an insulating state consistent with experimentally determined insulators  $\text{Sr}_2\text{CrReO}_6$ ,  $\text{Ca}_2\text{CrReO}_6$ , and  $\text{Ca}_2\text{FeReO}_6$ . The threshold value of  $U_{\text{Re}}$  for orbital ordering is reduced by inducing  $E_g$  octahedral distortions of the same C-type wavelength (denoted COD), which serves as a structural signature of the orbital ordering; octahedral tilting also reduces the threshold. The COO, and the concomitant COD, are a spontaneously broken symmetry for the Sr based materials (i.e.  $a^0a^0c^-$  tilt pattern), while not for the Ca based systems (i.e.  $a^-a^-b^+$  tilt pattern). Spin-orbit coupling does not qualitatively change the physics of the COO/COD, but can induce relevant quantitative changes. We prove that a single set of  $U_{\text{Cr}}, U_{\text{Fe}}, U_{\text{Re}}$  capture the experimentally observed metallic state in  $\text{Sr}_2\text{FeReO}_6$  and insulating states in the other three systems. We predict that the COO is the origin of the insulating state in  $\text{Sr}_2\text{CrReO}_6$ , and that the concomitant COD may be experimentally observed at sufficiently low temperatures (ie. space group  $\text{P}4_2/m$ ). Additionally, given our prescribed values of  $U$ , we show that the COO induced insulating state in  $\text{Ca}_2\text{CrReO}_6$  will survive even if the COD amplitude is suppressed (e.g. due to thermal fluctuations).

PACS numbers: 71.30.+h, 75.70.Cn, 75.47.Lx, 75.25.Dk, 71.15.Mb

## I. Introduction

### A. General Background

There is a huge phase space of possibilities for perovskite based transition metal oxides with more than one type of transition metal which nominally bears  $d$  electrons, and experimental efforts are continuing to expand in this direction; including chemical synthesis [1–5] and layer-by-layer growth by pulsed laser deposition [4, 6, 7]. Given that many of these materials will exhibit strongly correlated electron behavior, it will be critical to have appropriate first-principles based approaches which can be applied to this vast phase space in order to guide experimental efforts; allowing for the development of novel, functional materials. Nearly two decades ago, room-temperature ferrimagnetism (sometimes loosely referred to as ferromagnetism) was discovered in the double-perovskite (DP) transition metal oxides (TMO)  $\text{Sr}_2\text{FeMoO}_6$  [8], attracting much attention to DP TMO's due to their rich physics and potential for spintronic applications [4].

Among the various double perovskites, Re-based DPs are a particularly intriguing class; and the small set  $A_2B\text{ReO}_6$  ( $A=\text{Sr}, \text{Ca}$  and  $B=\text{Cr}, \text{Fe}$ ) already contains a wealth of interesting physics and impressive metrics. Moreover, this particular set of Re-based DPs materials forms a sort of family which descends from the same low energy Hamiltonian of Re dominated orbitals, de-

spite the fact that Cr and Fe have different numbers of electrons; and this can be deduced from nominal charge counting along with some amount of post facto knowledge (see Section III A for a more detailed explanation). Given that Sr and Ca are isovalent (ie. nominally  $2+$ ), these two cations serve as binary parameter to modify the degree and type of octahedral tilting, changing the bandwidth of the system. Switching between Cr and Fe changes the valence by two electrons and alters the  $B$  site energy. However, Cr and Fe are totally analogous in the sense that both yield a filled spin shell given a predominant octahedral crystal field and a high spin configuration (ie.  $t_{2g,\uparrow}^3$  and  $t_{2g,\uparrow}^3e_{g,\uparrow}^2$ , respectively). Experiment dictates that the resulting four permutations yield both metallic and insulating ground states, insulator to metal transitions as a function of temperature (for reasonable temperature scales), structural transitions as a function of temperature, and in some cases very high ferrimagnetic to paramagnetic transition temperatures. Moreover, this Re-based family of DP contains unexplained phenomena, such as the discontinuous, isostructural phase transition in  $\text{Ca}_2\text{FeReO}_6$ . Therefore, there are a variety of phenomenological, qualitative, and quantitative challenges which need to be addressed in this family.

Given that all of these compounds are strongly magnetically ordered at low temperatures, it is reasonable to expect that DFT+ $U$  might provide an overarching, qualitative view of the physics; perhaps even quantitative. In this work, we use DFT+ $U$  calculations to investigate the electronic and structural aspects of  $A_2B\text{ReO}_6$

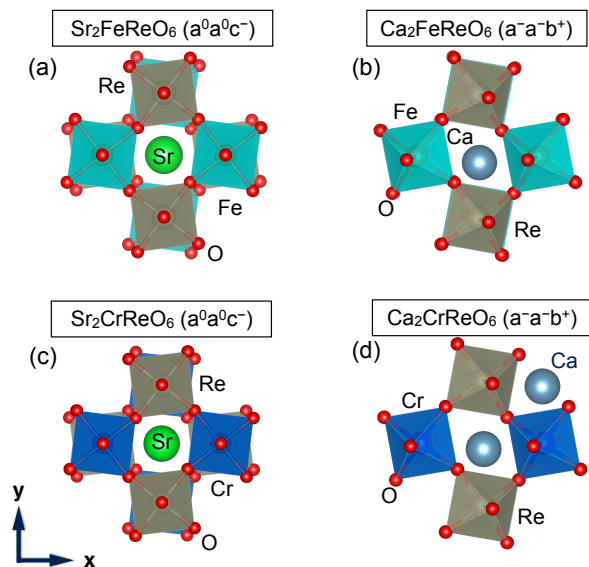


FIG. 1: Orthographic view of the crystal structures of (a)  $\text{Sr}_2\text{FeReO}_6$ , (b)  $\text{Ca}_2\text{FeReO}_6$ , (c)  $\text{Sr}_2\text{CrReO}_6$ , and (d)  $\text{Ca}_2\text{CrReO}_6$ . The octahedral tilt pattern is listed in each case.

( $A=\text{Sr}$ ,  $\text{Ca}$ , and  $B=\text{Cr}$ ,  $\text{Fe}$ ), systematically accounting for the effects of octahedral distortions and rotations; in addition to carefully exploring the effect of the Hubbard  $U$  for both the  $B$  sites and  $\text{Re}$ . We show that a single set of  $U_{\text{Re}}, U_{\text{Fe}}, U_{\text{Cr}}$  can obtain qualitative agreement with known experiments of all four compounds. Particular attention is paid to isolating the effects of the Hubbard  $U$  by additionally considering cubic reference structures in the absence of any octahedral distortions or tilting. Finally, we explore the effect of spin-orbit coupling, demonstrating that it can perturb the COO and the resulting COD, but the qualitative trends hold.

### B. Literature review of $A_2B\text{ReO}_6$ ( $A=\text{Sr}$ , $\text{Ca}$ and $B=\text{Cr}, \text{Fe}$ )

Here we review the experimental literature, in addition to some of the theoretical literature, on our  $\text{Re}$ -based compounds of interest:  $A_2B\text{ReO}_6$  ( $A=\text{Sr}$ ,  $\text{Ca}$ , and  $B=\text{Cr}$ ,  $\text{Fe}$ ). All four compounds form a perovskite structure with the  $\text{Re}/B$  atoms ordering in a  $\vec{q} = (\frac{1}{2}, \frac{1}{2}, \frac{1}{2})$  motif (with respect to the primitive perovskite lattice vectors); and all systems are ferrimagnetically ordered below room temperature with the  $\text{Re}$  and  $B$  atoms having opposite spins. We begin by presenting an experimental table of the crystal structures for the ground state and at temperatures above the structural transition; except for  $\text{Ca}_2\text{CrReO}_6$ , which is not known to have a transition near room temperature (see Table I). Additionally, we tabulate the transition temperature and the nature of the ground state (i.e. metal vs. insulator). We will also dis-

uss other experimental viewpoints from the literature, some with dissenting views, that are not represented in this table.

Bulk  $\text{Sr}_2\text{FeReO}_6$  is tetragonal at 5K ( $I4/m$ , space group 87) as shown in Fig. 1(a), metallic (even in well ordered samples)[1, 2, 9, 10], has  $a^0a^0c^-$  octahedral tilting, and in-plane and out-of-plane  $\angle\text{Fe-O-Re}$  are  $171.9^\circ$  and  $180^\circ$ , respectively [2]. Upon increasing temperature, it undergoes a tetragonal-to-cubic phase transition at  $T_t = 490\text{K}$  to space group 225 ( $Fm\bar{3}m$ ), removing octahedral tilting.

$\text{Ca}_2\text{FeReO}_6$  is monoclinic at 7K ( $P2_1/n$ , space group 14-2), and has  $a^-a^-b^+$  octahedral tilting (see Fig. 1(b)). It is generally known as insulator at low temperature [1, 10–12], though Fisher *et al.* suggested that it may be a bad metal [13]. With increasing temperature,  $\text{Ca}_2\text{FeReO}_6$  undergoes a concomitant structural and metal-insulator transition (MIT) at 140K [11, 12]. Interestingly, the structures above and below the transition have the same space group symmetry, and octahedral tilting, but the structural parameters are slightly different [12]. Based on the experimental results, we infer that the predominant structural change at the phase transition is the enhancement and reorientation of a local axial octahedral distortion of the  $\text{Re-O}$  octahedron (i.e. linear combinations  $A_{1g} + E_g$  octahedral modes, as defined from the cubic reference) which order in an C-type antiferro (i.e.  $\vec{q} = (0, \frac{1}{2}, \frac{1}{2})$ ) manner (with respect to the primitive face-centered cubic lattice vectors of the double perovskite); we refer to this as an C-type octahedral distortion (COD) (see Table V for projections onto the octahedral mode amplitudes). The COD will be demonstrated to be a signature of orbital ordering of the  $\text{Re}$  electrons; which we will prove to be the common mechanism of the MIT in this entire family of materials. The COD is not a spontaneously broken symmetry in this space group (e.g. there is a small non-zero amplitude in the high temperature phase), and there are two symmetry inequivalent variants (i.e.  $\text{COD}^+$  and  $\text{COD}^-$ , see Fig. 10) which represent the low and high temperature structures, respectively. Incidentally, the COD is a spontaneously broken symmetry in the  $\text{Sr}$ -based crystals (due to the  $a^0a^0c^-$  tilt pattern), whereby  $\text{COD}^+$  and  $\text{COD}^-$  are identical by symmetry.

In order to clearly characterize the COD, the bond lengths of the  $\text{Re-O}$  octahedron from the experimental structures are summarized in Fig. 9. Above the structural transition, the  $\text{Re-O}$  bonds are split into three sets of two equal bond lengths (where the equal bonds arise from the inversion symmetry at the  $\text{Re}$  site), but two of the three sets are very similar. Specifically, at  $T=300\text{K}$   $d_{\text{Re1-O1}} = 1.959$ ,  $d_{\text{Re1-O2}} = 1.954$ , and  $d_{\text{Re1-O3}} = 1.939$ , where  $\text{Re1-O1}$  and  $\text{Re1-O2}$  are approximately within the  $a-b$  plane and  $\text{Re1-O3}$  is approximately along the  $c$ -axis (see Fig. 4, panels c and d). In order to quantify relevant aspects of the octahedral distortions, we will define a parameter  $d_{|x-y|} = |d_{\text{Re-O1}} - d_{\text{Re-O2}}|$ , which is small in the high temperature phase (i.e.  $d_{|x-y|} = 0.005\text{\AA}$

at  $T=300\text{K}$ ); and  $d_{|x-y|}$  is precisely the amplitude of the  $E_g^{(0)}$  octahedral mode in the unrotated local coordinate system. For the symmetry equivalent Re within the unit cell (i.e. Re2), the nearly equivalent O1 and O2 bond lengths are swapped (i.e.  $d_{|x-y|}$  is identical but the direction of the long/short bonds have reversed); while Re-O3 is identical. Upon changing to the low temperature phase, there is a modest change whereby the Re-O3 bond length shifts up by  $0.006\text{\AA}$  (i.e. equivalently in both Re), and a more dramatic change whereby the splitting between Re-O1 and Re-O2 becomes substantially larger (i.e.  $d_{|x-y|} = 0.014\text{\AA}$ ). As in the high temperature structure, symmetry dictates that the direction of  $d_{|x-y|}$  alternates between the two Re sites. The main difference is that  $d_{|x-y|}$  acquires an appreciable value in the low temperature phase, and the COD switches between  $\text{COD}^+$  and  $\text{COD}^-$  (see Section III B 3 for a more detailed discussion).

Interestingly, Granado *et al.* suggested that there is phase separation between 10K and 650K, with all three phases being monoclinic [14]. More specifically, the most abundant phases are found to be the M1 and M2 phases, with fraction of 55% and 45%, respectively, and the main differences between the two phases are the  $b$ -lattice parameter and angle  $\beta$ . Similarly, Westerburg *et al.* also observed two different phases below 300K [15]. We note that the M1 and M2 phases in Granado *et al.*'s results [14] are similar to the low- $T$  and high- $T$  phases reported by Oikawa *et al.*, where the separation was not detected [12]. M1, which has the largest portion at low temperature, has a  $b$  lattice parameter which is  $\sim 0.015\text{\AA}$  smaller and a  $\beta$  which is  $\sim 0.1^\circ$  larger than those of the M2 phase, which constitutes  $\sim 90\%$  of the high  $T$  phase [14]. Similarly, at 140K, the low- $T$  phase has smaller  $b$  and larger  $\beta$  than the high- $T$  phase in Oikawa *et al.*'s report [12].

Having clarified the nature of the experimentally measured structural distortions in  $\text{Ca}_2\text{FeReO}_6$ , we return to the issue of the MIT as addressed in the literature. Since there are nominally only Re  $t_{2g}$  states near the Fermi level, the MIT is a gapping of these states. Oikawa *et al.* suggested that the  $d_{xy}+d_{yz}$  and  $d_{xy}+d_{zx}$  orbitals are randomly arranged at Re sites in the metallic phase, whereas the  $d_{yz}+d_{zx}$  orbitals are preferentially occupied in the insulating phase; and the splitting between  $d_{yz}+d_{zx}$  and  $d_{xy}$  orbitals produce the energy gap [12]. Previous local spin density functional theory (LSDA) studies showed that  $\text{Ca}_2\text{FeReO}_6$  is metallic without considering on-site Coulomb repulsion  $U$  term for Re ( $U_{\text{Re}}$ ) [16, 17] and a gap is opened with the large value  $U=3-4$  eV [11, 18].

Gong *et al.* concluded that the Re  $t_{2g}$  states order into a  $d_{xy}+d_{zx}$  configuration using the modified Becke-Johnson (mBJ) exchange-correlation potential, and showed that  $\text{Ca}_2\text{FeReO}_6$  is insulating; though this study did not explicitly identify the C-type orbital ordering that drives this insulating state. A noteworthy approximation made in their work is that the atomic coordinates are relaxed within GGA, where  $d_{|x-y|}$  is only  $0.004\text{\AA}$ , which is far smaller than low temperature ex-

TABLE I: Symmetries of the Re-DPs at low temperature (i.e.  $\leq 10\text{K}$ ) and above the respective transition temperature; structural phase transition temperature ( $T_t$ ); and the nature of the electronic ground state.

Materials	low $T$	high $T$	$T_t$	M/I
$\text{Sr}_2\text{FeReO}_6$	$I4/m$ <sup>a</sup>	$Fm\bar{3}m$ <sup>a</sup>	490 K <sup>a</sup>	metal
$\text{Ca}_2\text{FeReO}_6$	$P2_1/n$ <sup>b,d</sup>	$P2_1/n$ <sup>d</sup>	140 K <sup>d</sup>	insulator
$\text{Sr}_2\text{CrReO}_6$	$I4/m$ <sup>a</sup>	$Fm\bar{3}m$ <sup>a,c</sup>	260 K <sup>a</sup>	insulator*
$\text{Ca}_2\text{CrReO}_6$	NA	$P2_1/n$ <sup>b</sup>		insulator

\* recent experiment shows fully ordered film is insulating [3]

<sup>a</sup> ref. [2]

<sup>b</sup> ref. [1]

<sup>c</sup> ref. [20]

<sup>d</sup> ref. [12]

perimental value in the insulating state. The importance of this amplified COD amplitude will be clearly demonstrated within our work.

Antonov *et al.*[19] reported the electronic structure of  $\text{Ca}_2\text{FeReO}_6$  using LSDA+ $U$ +spin-orbit-coupling calculations. Using structures obtained from experiment at different temperatures, which encompasses the discontinuous phase transition at  $T=140\text{K}$  [12], they showed that spin and orbital moments also have abrupt changes across the transition, while both change linearly with structures from temperatures below and above the MIT [19].

$\text{Sr}_2\text{CrReO}_6$  has been determined to be tetragonal with an  $a^0a^0c^-$  octahedral tilt pattern (i.e. space group  $I4/m$ , see Fig. 1(c))[1, 2]. Teresa *et al.* reported a structural transition at  $T = 260\text{K}$ , going from  $I4/m$  to  $Fm\bar{3}m$  (with increasing temperature) whereby the octahedral tilts and the tetragonality are disordered. Alternatively, Kato *et al.* found that  $\text{Sr}_2\text{CrReO}_6$  is still  $I4/m$ [1, 21] at room temperature, implying that the transition temperature was even higher in these particular samples; while Winkler *et al.* found that it was cubic ( $Fm\bar{3}m$ ) at room temperature[20]. This is likely a minor discrepancy given that the structure measured by Kato *et al.* at room temperature (300K) only has small deviations from  $Fm\bar{3}m$ : the in-plane Cr-O-Re angle in the tetragonal structure is  $179.7^\circ$ , close to  $180^\circ$ , and the lattice parameters are nearly cubic with  $\sqrt{2}a=7.817$  and  $c=7.809$   $\text{\AA}$ [1].

Recent experiments have found  $\text{Sr}_2\text{CrReO}_6$  to be insulating at low temperatures, in contrast with earlier work which found metallic states. Specifically, Hauser *et al.* found that a  $\text{Sr}_2\text{CrReO}_6$  film grown on STO, where the strain is less than 0.05%, is insulating at 2K with a 0.21eV energy gap [3]. Alternatively, numerous samples obtained from chemical synthesis were all found to be metallic [1, 2, 20, 21], in addition to previous thin film samples[22]. It should be noted that Kato *et al.* emphasized that  $\text{Sr}_2\text{CrReO}_6$  is a very bad metal, and lies at the vicinity of a Mott-insulating state [21]. Moreover, Hauser *et al.* suggested that oxygen vacancies are the reason why  $\text{Sr}_2\text{CrReO}_6$  samples reported in previous studies were half-metallic [23, 24]. Indeed, previously reported

metallic  $\text{Sr}_2\text{CrReO}_6$  samples have a large amount of defects, such as Cr/Re anti-site defect: 9% [25], 15% [26], 10–12% [2], and 23.3% [1]. However, there is not yet theoretical justification for why  $\text{Sr}_2\text{CrReO}_6$  might be an insulator. Unfortunately, full structural parameters have not yet been extracted from the insulating film at low temperatures [3], which could reveal signatures of an orbitally ordered insulator which we predict in our analysis (see Section III B 2).

To our knowledge, there are only few experiments on  $\text{Ca}_2\text{CrReO}_6$  [1, 21]; finding a monoclinic crystal structure (space group  $P2_1/n$ , see Fig. 1(d)) and an insulating ground state. The energy gap is not reported yet, though the reflectivity spectra and optical conductivity were measured [21]. Theoretically, the recent mBJ study of Gong *et al.* suggested that the energy gap is 0.38eV, much larger than that of  $\text{Ca}_2\text{FeReO}_6$ . The resistivity curve suggests that it is still insulating at room temperature, but the resistivity will have an error given the 12-13.7% of B-site disorder [1, 21], similar to the case of  $\text{Sr}_2\text{CrReO}_6$ . In addition, structural parameters as a function of temperature have not yet been reported, which will be relevant to testing the predictions in our study.

In the existing literature, the effect of electronic correlation, orbital ordering, and octahedral distortions have not been sufficiently isolated to give a universal understanding of this family. Most importantly, the origin of the MIT and its relation to orbital ordering and the concomitant COD have not been elucidated. Theory and computation will be critical to separating cause from effect.

### C. Orbital ordering

Orbital ordering is a well known phenomena in transition metal oxides [27–29], and it can drive a material into an insulating ground state. Classic examples which display antiferro orbital ordering include the  $3d^9$  perovskite  $\text{KCuF}_3$  with ordering of  $e_g$  electrons [30], the  $3d^1$  ( $t_{2g}$ ) perovskites  $\text{LaTiO}_3$  and  $\text{YTiO}_3$  [31, 32], and the  $3d^4$  perovskite  $\text{LaMnO}_3$  [33]. It is useful to compare the Re-based DP's to these classic examples to provide context for the orbital ordering we identify in this study.

Two main mechanisms which drive orbital ordering are the electron-lattice ( $e-l$ ) coupling, with a very relevant scenario being the well known Jahn-Teller (JT) Effect, and electron-electron ( $e-e$ ) interactions. Disentangling these two effects can be complicated. In the context of DFT+ $U$  calculations, the Hubbard  $U$  captures a very relevant portion of the  $e-e$  interactions which drive orbital ordering; similar to the  $U$  in a model Hamiltonian which gives rise to superexchange [27]. The  $e-l$  coupling is accounted for in the DFT portion of the calculation (assuming a local or semi-local approximation to the DFT functional). If experimentally deduced orbital ordering is not found at the level of DFT (ie.  $U=0$ ), then  $e-e$  interactions are likely playing a dominant role; while if DFT

does predominantly capture the orbital ordering, then the  $e-l$  coupling is likely playing a dominant role. Generally, the  $e-l$  coupling in the JT effect is much larger for scenarios involving  $e_g$  electrons as compared to  $t_{2g}$ .

In the aforementioned classic examples of orbital ordering involving  $e_g$  electrons, important contributions are realized from both  $e-e$  interactions and  $e-l$  coupling. In  $\text{LaMnO}_3$ , an antiferro Jahn-Teller distortion, and corresponding orbital ordering, is found even at the level of GGA (ie.  $U_{\text{Mn}}=0$ ), though a non-zero  $U_{\text{Mn}}$  is needed to properly capture the orbitally ordered state [33]. A similar scenario arises for  $\text{KCuF}_3$ , where GGA weakly predicts an antiferro Jahn-Teller distortion that is observed in experiment (ie. the stabilization energy is grossly underestimated while the distortion magnitude is too small), whereas including the on-site  $U$  gives reasonable quantitative agreement with experiment (both within DFT+ $U$  and DFT+DMFT) [30, 34, 35]. Alternatively, if one remains in the cubic reference structure, preventing coupling with the lattice, an on-site  $U$  of 7eV can drive the orbitally ordered insulator with a corresponding transition temperature of roughly 350K [30]. Therefore, both mechanism can drive the same instability, but in isolation the on-site  $U$  recovers a much larger component of temperature required for the MIT; though both ingredients are necessary to quantitatively describe experiment.

The other interesting scenario pertains to orbital ordering in  $t_{2g}$ -based orbitals, where the  $e-e$  interactions are expected to be the primary origin of the orbital ordering given the relatively weak  $e-l$  coupling of  $t_{2g}$ -based states. Two important materials which exhibit this scenario are  $\text{YTiO}_3$  and  $\text{LaTiO}_3$ . In  $\text{YTiO}_3$ , theoretical works which incorporate orbital ordering successfully explain physical properties such as the ferromagnetic ground state [31, 32, 36–38]. Experimentally, the polarized neutron diffraction technique [39], nuclear magnetic resonance (NMR) spectra [40, 41], x-ray linear dichroism [42], and resonant x-ray scattering [43] support orbital ordering in  $\text{YTiO}_3$ . While the presence of orbital ordering is well accepted, the overall mechanism is still under debate [31, 32, 36]. A JT-based model was used to explain the physical properties such as the ferromagnetic ordering [37, 38, 44, 45], though Raman and resonant inelastic x-ray scattering spectra have been successfully explained by the  $e-e$  induced superexchange [36, 43]. In addition, a Wannier analysis of the Kohn-Sham Hamiltonian demonstrated that the JT effect is not a predominant influence [32]. While the ground state of  $\text{LaTiO}_3$  is less well established, orbital ordering is supported by x-ray and neutron-diffraction studies [46], temperature dependent structural changes [47], Raman shifts [48], specific heat measurements [49], and thermal conductivity measurements [45].

The orbital ordering which we identify in the  $3d-5d$  Re-based DP's of this study has a number of distinct circumstances as compared to these classic  $3d$  single perovskites. First, in the Re-DP's the magnetic transition temperature ( $T_c$ ) is much higher than the metal-insulator transi-

tion temperature ( $T_{\text{MIT}}$ ), whereas the reverse is true in the single  $3d$  perovskites. In  $\text{LaTiO}_3$ , the Néel temperature  $T_N$  is 146K and it is still insulating at 300K[46, 50]. In  $\text{YTiO}_3$ , the Curie temperature is  $T_C=30\text{K}$  and it remains insulating at room temperature[42, 51, 52]. Recall that in  $\text{KCuF}_3$   $T_N=38\text{K}$  [53] while the JT distortion and orbital ordering is stable beyond 800K[54, 55]. In  $\text{LaMnO}_3$ ,  $T_N$  is 140K in [56] while the JT transition and orbital ordering is stable until 750K[57]. Alternatively, in  $\text{Ca}_2\text{FeReO}_6$  the ferrimagnetic transition temperature  $T_C=520\text{K}$ , which is much higher than  $T_{\text{MIT}}=140\text{K}$ , opposite to the classic  $3d$  perovskites.

Another difference is that the electronic structure of the  $3d$ - $5d$  DPs are generally governed by  $5d$  orbitals, which may have a non-trivial spin-orbit interaction[58]. While  $5d$  orbitals are more delocalized than  $3d$  orbitals, it should be kept in mind that the rock salt ordering of the DP's results in relatively small effective Re bandwidths (see Section III A).

A well studied class of DP's where orbital ordering may be relevant is the  $A_2BB'O_6$  double perovskites, where  $B$  has fully filled or empty  $d$  orbital and  $B'$  is a  $5d$  transition metal. One well studied type of family is the  $B'=5d^1$  Mott insulators, such as  $\text{Ba}_2\text{BOsO}_6$  ( $B=\text{Li, Na}$ ) [58–66] and  $\text{Ba}_2\text{BMoO}_6$  ( $B=\text{Y, Lu}$ ) [61]. These materials have very weak magnetic exchange interactions (e.g.  $T_C$  of  $\text{Ba}_2\text{NaOsO}_6$  is 6.8-8 K [59, 60]), and exotic phases have been proposed such as quantum-spin-liquids, valence-bond solids, or spin-orbit dimer phases[58, 63]. Xiang *et al.* [62] studied  $\text{Ba}_2\text{NaOsO}_6$  using the first-principles calculations, and suggested that an insulating phase cannot be obtained within GGA+ $U$  up to  $U - J=0.5$  Ryd: orbital ordering is not observed in their electronic band structure within GGA+ $U$ . They also show that  $\text{Ba}_2\text{NaOsO}_6$  is insulating within GGA+ $U$  when including spin-orbit coupling (SOC) with  $U - J=0.2\text{Ryd}$  and the [111] magnetization axis. Gangopadhyay *et al.* [65, 66] also proposed that SOC is essential to obtain a nonzero band gap, using hybrid functional + SOC calculations. Based on experiment, Erickson *et al.* proposed that  $\text{Ba}_2\text{NaOsO}_6$  has orbital ordering with a nonzero wavevector, deduced in part from the small negative Weiss temperature from magnetic susceptibility measurements [59].

Another analogous example is Ir-based double perovskite  $\text{Sr}_2\text{CeIrO}_6$ , where Ce has a filled shell and the Ir  $5d$  nominally have 5 electrons (or one hole) in the  $e_g^\pi + a_{1g}$  orbitals (ie. descendants of  $t_{2g}$ )[67], and this results in weak antiferromagnetic coupling (ie.  $T_N=21\text{K}$ ). Additionally, orbital ordering has been identified in this material, where the hole orders in the  $e_g^\pi$  shell among the  $d_{xz}$  and  $d_{yz}$  orbitals with an antiferromagnetic modulation; and it is accompanied by a structural distortion. The authors attribute the orbital ordering to the Jahn-Teller effect, though they demonstrate the  $U_{\text{Ir}}$  is a necessary condition for opening a band gap. It should be noted that the wavevector of the antiferro orbital and structural ordering in this system is the same as what we

identify in the Re-based family in the present work.

Re-based double perovskites are quiet distinct from the aforementioned double perovskites with empty or fully filled  $d$  shell on the  $B$  ion. Unlike these latter materials, Re-based DPs have nonzero magnetic spin for  $B$  (e.g., Cr has spin 3/2 and Fe has spin 5/2), and thus have strong a strong antiferromagnetic exchange interaction between  $B$  and  $B'$ ; resulting in a  $T_C$  that is much higher than room temperature (e.g.  $T_C$  in  $\text{Sr}_2\text{CrReO}_6$  is 600K). Therefore, the spin degrees of freedom are locked in until relatively high temperatures, creating an ideal testbed to probe orbital physics. The family of Re-based DP's evaluated in this study are ideally distributed in parameter space about the orbital ordering phase transition.

## II. Computation Details

We used the projector augmented wave (PAW) method [68, 69] in order to numerically solve the Kohn-Sham equations, as implemented in the VASP code [70]. The exchange-correlation functional was approximated using the revised version of the generalized gradient approximation (GGA) proposed by Perdew *et al.* (PBEsol) [71]. In all cases, the spin-dependent version of the exchange correlation functional is employed. A plane wave basis with a kinetic energy cutoff of 500 eV was employed. We used a  $\Gamma$ -centered  $\mathbf{k}$ -point mesh of  $9 \times 9 \times 7$  ( $11 \times 11 \times 9$  for density of states). Wigner-Seitz radii of 1.323, 1.164, and 1.434 Å were used for site projections on Cr, Fe and Re atoms, respectively, as implemented in the VASP-PAW projectors.

The GGA+ $U$  scheme within the rotationally invariant formalism and the fully localized limit double-counting formula [34] is used to study the effect of electron correlation. The electronic and structural properties critically depend on  $U_{\text{Re}}$ , and therefore we carefully explore a range of values. We also explore how the results depend on  $U_{\text{Cr}}$  and  $U_{\text{Fe}}$ , which play a secondary but relevant role in the physics of these materials. We do not employ an on-site exchange interaction  $J$  for any species, as this is already accounted for within the spin-dependent exchange-correlation potential [72, 73]. A post facto analysis of our results demonstrate that a single set of values (which are reasonable as compared to naive expectations and previous work) can account for the electronic and crystal structure of this family (see Section III D), and it is useful to provide this information at the outset for clarity. In the absence of spin-orbit coupling, values of  $U_{\text{Fe}}=4$  eV,  $U_{\text{Cr}}=2.5$  eV, and  $U_{\text{Re}}=2$  eV are found; including spin-orbit coupling requires  $U_{\text{Re}}$  to be slightly decreased to 1.9 eV in order to maintain the proper physics. In subsequent discussions, the units of  $U$  will always be in electron volts (eV), and this may be suppressed for brevity.

We used experimental lattice parameters throughout (see Table I), and the reference temperature is 300K unless otherwise specified. Atomic positions within the unit cell were relaxed until the residual forces were less than

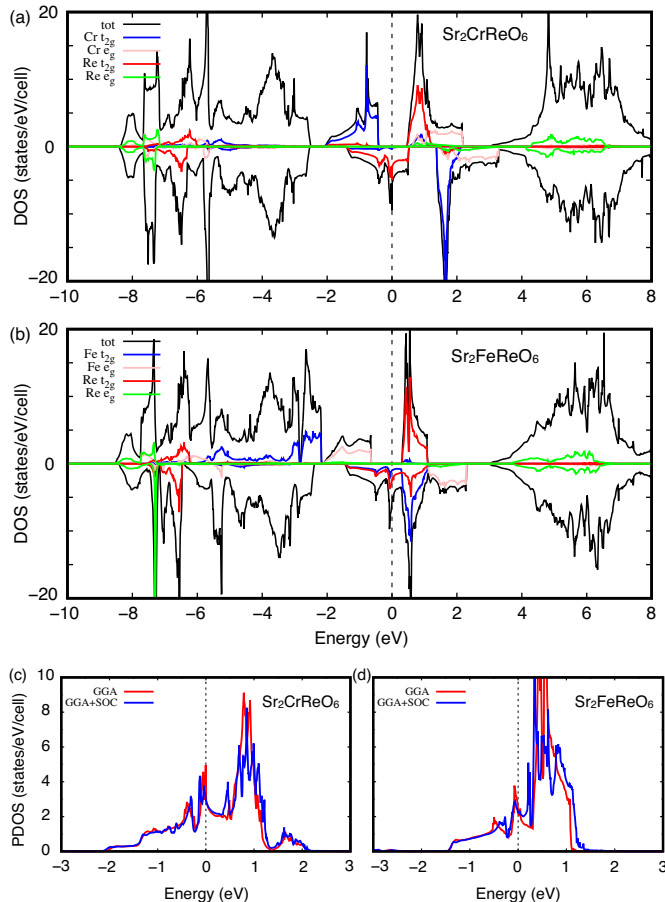


FIG. 2: (a),(b) Total and atom/orbital projected spin-resolved density of states (DOS) from DFT for (a)  $\text{Sr}_2\text{CrReO}_6$  and (b)  $\text{Sr}_2\text{FeReO}_6$ . The majority spin are shown as a positive DOS while the minority are negative. Orbital projections are given for  $t_{2g}$  and  $e_g$  states for Re, Fe, and Cr. (c),(d) Illustrating the effect of spin-orbit coupling in the Re Projected density of states, comparing GGA (red solid line) and GGA+SOC (blue solid line) for (c)  $\text{Sr}_2\text{CrReO}_6$  and (d)  $\text{Sr}_2\text{FeReO}_6$ . For GGA, majority and minority spins are summed for comparison. The Fermi energy is zero in all panels, and  $Fm\bar{3}m$  is used throughout.

0.01 eV/Å. In select cases we do relax the lattice parameters as well to ensure no qualitative changes occur, and indeed the changes are small and inconsequential in all cases tested.

### III. Results and discussion

#### A. General Aspects of the Electronic Structure

We begin by discussing the nominal charge states of the transition metals, the basic energy scales, and the common mechanism of the metal-insulator transition in these compounds; which is a C-type antiferro orbital ordering.

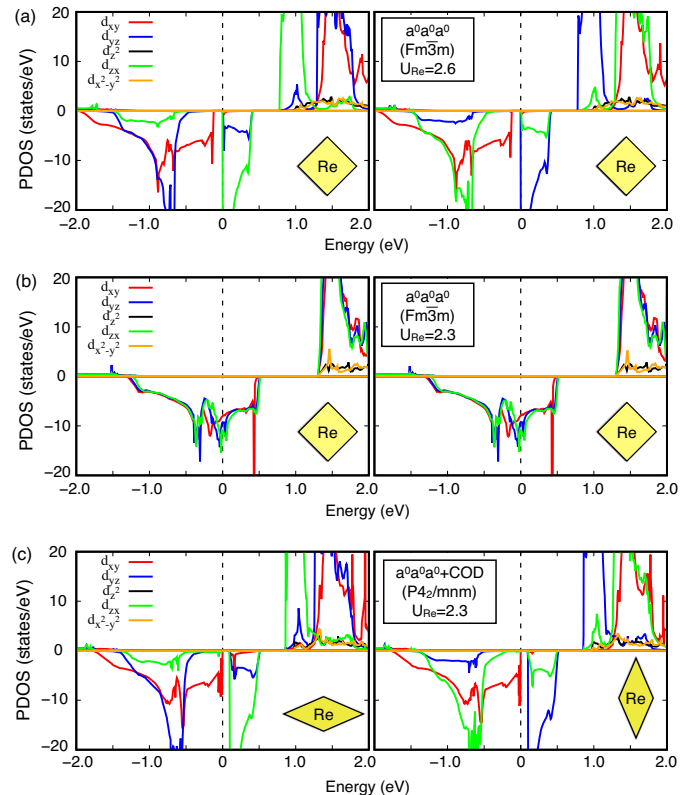


FIG. 3: Re projected density of states (PDOS) for  $\text{Sr}_2\text{CrReO}_6$  within DFT+ $U$ . (a)  $Fm\bar{3}m$  crystal structure and  $U_{\text{Re}}=2.6$ , resulting in an orbitally ordered insulator. (b)  $Fm\bar{3}m$  crystal structure and  $U_{\text{Re}}=2.3$ , resulting in a metal. (c)  $P4_2/mnm$  crystal structure (ie.  $a^0a^0a^0$  tilt, with COD) and  $U_{\text{Re}}=2.3$ , resulting in an orbitally ordered insulator.  $U_{\text{Cr}}=0$  in all cases.

A perfect cubic structure ( $Fm\bar{3}m$ ) is first considered, in the absence of SOC (which will be addressed at the end of this discussion). Given the Re double perovskite  $A_2B\text{ReO}_6$  ( $A=\text{Sr,Ca}$ ,  $B=\text{Fe,Cr}$ ), nominal charge counting dictates that the transition metal pair  $B\text{Re}$  must collectively donate 8 electrons to the oxygen (given that  $A_2$  donates 4 electrons), and it is energetically favorable (as shown below) to have  $\text{Re}^{5+}$  ( $d^2$ ) and  $B^{3+}$  ( $\text{Cr} \rightarrow d^3$  and  $\text{Fe} \rightarrow d^5$ ) in a high spin configuration. The Re spin couples antiferromagnetically to the  $B$  spin via superexchange, yielding a ferrimagnetic state. Given that the nominally  $d^5$  Fe has a half filled shell when fully polarized, and that the nominally filled  $d^3$  Cr has a half-filled  $t_{2g}$ -based shell when fully polarized, none of these compounds would be expected to have Fe or Cr states at the Fermi energy when strongly polarized. Given that Re is in a  $d^2$  configuration, group theory dictates that the system will be metallic with majority spin Re states present at the Fermi energy within band theory.

These naive expectations are clearly realized in DFT calculations (ie.  $U=0$ ), as illustrated in  $\text{Sr}_2\text{CrReO}_6$  and

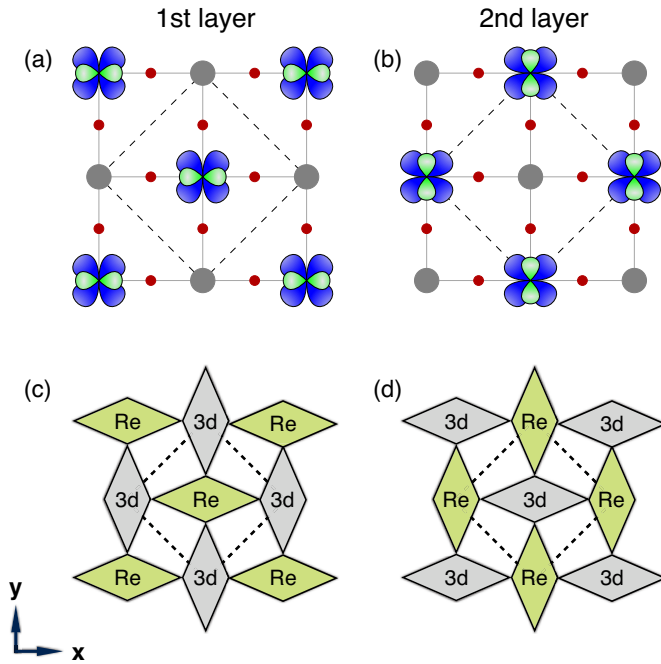


FIG. 4: Schematic diagrams of the C-type orbital ordering for the 1st and 2nd layer along the  $c$ -axis of the conventional cubic cell, shown in panels (a) and (b), respectively. Red dots correspond to oxygen atoms while grey dots correspond to  $B$  atoms (ie. Cr or Fe). The pictured  $t_{2g}$  orbitals are located on Re sites. Panels (c) and (d) depict a schematic of the COD type structural distortion, whereby each local octahedron is distorted in a positive or negative  $E_g^{(0)}$  distortion. Positive  $E_g^{(0)}$  corresponds to the elongation along the  $y$ -direction and contraction along the  $x$ -direction (see Ref. [74] for formula). Dotted lines correspond to the unit cell.

$\text{Sr}_2\text{FeReO}_6$  using the  $Fm\bar{3}m$  structure (see Figure 2). It is useful to compare the Re states crossing the Fermi energy, which are substantially narrower for  $\text{Sr}_2\text{CrReO}_6$  as compared to  $\text{Sr}_2\text{FeReO}_6$ . Relatedly, the Cr states hybridize less with and are further from the Re states as compared to the case of Fe. The net result is that the Cr based compounds will have a smaller effective Re bandwidth, and therefore stronger electronic correlations which result in a higher propensity to form an insulating state.

At the level of  $\text{DFT}+U$ , or any static theory for that matter, one can only obtain an insulator from the fully spin-polarized scenario outlined above via an additional spontaneously broken symmetry, which could be driven either via the on-site Re Coulomb repulsion  $U_{\text{Re}}$ , structural distortions (which includes effects of electron-phonon coupling), or combinations thereof. As we will detail in the remainder of the paper, structural distortions alone (i.e. if  $U_{\text{Re}}=0$ ) cannot drive an insulating state in any of the four Re-based materials studied. Therefore, a non-zero  $U_{\text{Re}}$  is a *necessary condition* to drive the insulating state, but the minimum required

value of  $U_{\text{Re}}$  will be influenced by the details of the structural distortions; in addition to the on-site  $U$  of the  $3d$  transition metal and the SOC.

In order to illustrate the points of the preceding paragraph, we show that  $\text{DFT}+U$  calculations (with the only nonzero  $U$  being  $U_{\text{Re}}=2.6$ ) for  $\text{Sr}_2\text{CrReO}_6$  with the nuclei frozen in the  $Fm\bar{3}m$  structure results in a spontaneously broken symmetry of the electrons where the Re orbitals order and result in an insulating state (see Figure 3, panel a). We investigated ordered states consistent with  $q = (0, 0, 0)$ ,  $q = (0, 0, \frac{1}{2})$ ,  $q = (0, \frac{1}{2}, \frac{1}{2})$ , and  $q = (\frac{1}{2}, \frac{1}{2}, \frac{1}{2})$  (where  $q$  is a fractional coordinate of the reciprocal lattice vectors constructed from the primitive FCC DP lattice vectors); resulting in a ground state of  $q = (0, \frac{1}{2}, \frac{1}{2})$  (ie. C-type ordering). Specifically, a Re  $d_{xy}$  orbital is occupied on every site and there is a C-type alternation between  $d_{xz}$  and  $d_{yz}$  (see schematic in Figure 4, panels a and b). This C-type antiferro orbital ordering (denoted as COO) is generic among this  $A_2B\text{ReO}_6$  family. We will demonstrate that other orderings are possible and even favorable under certain conditions. For example, for small values of  $U_{\text{Re}}$ , the orbitals order in a ferro fashion (denoted FOO), whereby the  $d_{xy}$  and either the  $d_{xz}$  or  $d_{yz}$  is occupied at every Re site. For intermediate values of  $U_{\text{Re}}$ , a ferri version of the COO ordering (denoted FIOO) is found, though it is destroyed by octahedral tilts. These detailed scenarios are explored in Section III B.

We now turn to the importance of structural distortions, such as the  $E_g$  octahedral distortions which are induced by the orbital ordering. We first remain in the  $Fm\bar{3}m$  structure and lower the value of  $U_{\text{Re}}$  to  $2.3\text{eV}$ , demonstrating that the orbital ordering is destroyed and the gap is closed (see Figure 3, panel b). Subsequently, we allow any internal relaxations of the ions consistent with  $q = (0, 0, 0)$  or  $q = (0, \frac{1}{2}, \frac{1}{2})$ , demonstrating that an  $E_g^{(0)}$  octahedral distortion with C-type wavevector (denoted COD) condenses (see Figure 4 (c)/(d) for schematic); lowering the structural symmetry from  $Fm\bar{3}m$  to  $P4_2/mnm$  (see symmetry lineage in Figure 5) and allowing the COO to occur at  $U_{\text{Re}}=2.3\text{eV}$  (see Figure 3, panel c). This demonstrates how the COD can be an essential ingredient for realizing the orbitally ordered insulating state, by influencing the critical value of  $U_{\text{Re}}$  for the transition. Incidentally, it should be noted that when the orbital ordering changes, the structural distortion changes as expected. For example, ferro orbital ordering (ie. FOO) will lead to a ferro octahedral distortion (ie. FOD).

The above analysis proves that it is reasonable to characterize the insulating state as an orbitally ordered state, despite the fact that the COD structural distortion could play a critical role in moving the MIT phase boundaries to smaller values of  $U_{\text{Re}}$ . We will demonstrate that this renormalization of the critical  $U_{\text{Re}}$  via the COD allows a common value of  $U_{\text{Re}}$  to realize the insulating in  $\text{Sr}_2\text{CrReO}_6$ , while retaining a metallic state in  $\text{Sr}_2\text{FeReO}_6$ ; and we predict that the orbitally ordered

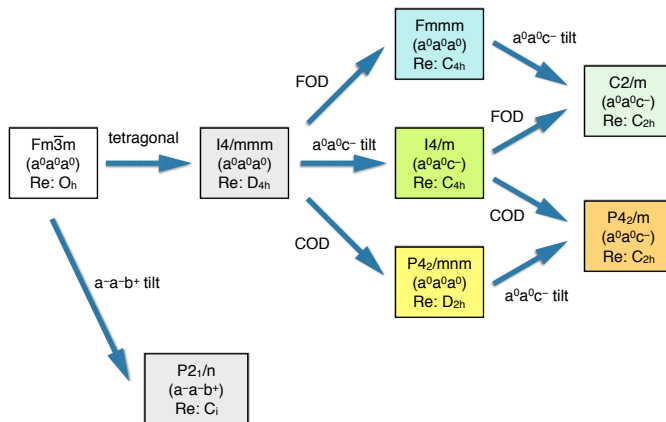


FIG. 5: Hierarchy of the  $A_2BB'O_6$  double perovskite space groups connected by various distortions, including octahedral tilts, FOD, and COD. The point group symmetry of the Re site is listed for all structures, along with the octahedral tilt pattern. Ca-based systems follow the  $a^-a^-b^+$  arrow, while Sr-based systems proceed along the tetragonal arrow.

state can persist in the near absence of the COD in  $\text{Ca}_2\text{CrReO}_6$  where electronic correlations are strongest. Given that the COD does not occur in the absence  $U_{\text{Re}}$ , we refrain from characterizing this as a Jahn-Teller effect, or pseudo Jahn-Teller effect in the case where the COO/COD is not a spontaneously broken symmetry, which could have been a primary driving force given the orbital degeneracy (or near degeneracy) present in these systems.

Another generic consideration is octahedral tilting, which will influence both the COO and the COD. The  $a^-a^-b^+$  tilt pattern of the Ca-based systems is a relatively large energy scale and therefore the tilts in these system exist independently of orbital ordering and or the COD. Alternatively, the  $a^0a^0c^-$  tilt pattern of the Sr-based systems is a much weaker energy scale, and therefore it may be somewhat coupled to the orbital ordering and the concomitant COD. These statements will be investigated in detail below (see Section III B), where we find that the differences of Sr/Ca are dominant over those of Fe/Cr in terms of setting the effective Re bandwidth; which results in a ordering of  $\text{Sr}_2\text{FeReO}_6$ ,  $\text{Sr}_2\text{CrReO}_6$ ,  $\text{Ca}_2\text{FeReO}_6$ ,  $\text{Ca}_2\text{CrReO}_6$  (smallest to largest effective Re bandwidth or electronic correlations).

Furthermore, the  $a^0a^0c^-$  tilt pattern may be isolated from the COO/COD as they break symmetry in a distinct manner (see symmetry lineage in Figure 5). Therefore, the COO/COD will be a spontaneously broken symmetry in the Sr based systems (should it occur). Alternatively, the  $a^-a^-b^+$  tilt pattern already has a sufficiently low symmetry such that the COO/COD is not a spontaneously broken symmetry. Therefore, the COD cannot strictly be a signature of orbital ordering in the case of the  $a^-a^-b^+$  tilt pattern. However, experiment

dictates that the magnitude of the COD is a useful metric given the discontinuous structural phase transition at 140K between two crystal structures of the same space group ( $P2_1/n$ , no. 14-2), whereby the magnitude of the COD changes discontinuously; and the variant switches from  $\text{COD}^+$  to  $\text{COD}^-$ .

Another generic consideration is the effect of the on-site Coulomb repulsion  $U$  for the  $3d$  transition metals, which do not nominally have states at low energies given the half filled (sub)shell of (Cr) Fe. However, in reality there is a non-trivial amount of  $3d$  states at low energies due to hybridization, more so for Fe than for Cr, and this determines the effective Re- $d$  bandwidth. While  $U_{\text{Re}}$  can drive orbital ordering even in the absence of  $U_{\text{Fe}}/U_{\text{Cr}}$ , as previously illustrated above (see Fig. 3), we will demonstrate the quantitative influence of  $U_{\text{Fe}}/U_{\text{Cr}}$  in renormalizing the critical value of  $U_{\text{Re}}$  for orbital ordering. First, considering  $U_{\text{Re}}=0$ , one can clearly see an unmixing of  $3d$  states from the Re- $d$  states as  $U_{\text{Fe}}/U_{\text{Cr}}$  is applied, further narrowing the effective Re- $d$  bandwidth (compare panels  $a \leftrightarrow c$  and  $e \leftrightarrow g$  in Fig. 6). This effect is more dramatic in the case of Fe, which started with a larger degree of hybridization. Focussing on the Fe compound, we see that applying  $U_{\text{Re}}=2$  does not drive the orbitally ordered insulator even when  $U_{\text{Fe}}=4$ , and thus the system remains metallic despite the diminished Re- $d$  bandwidth. Alternatively, when applying  $U_{\text{Re}}=2$  to the Cr compound, the addition of  $U_{\text{Cr}}=2.5$  is sufficient to move the critical value of  $U_{\text{Re}}$  below 2eV, and an orbitally ordered insulator is obtained. This demonstrates that, while indirect, the on-site  $U$  for the  $3d$  transition metal can play a critical role. Interestingly,  $U_{\text{Cr}}$  also turns out to be critical for stabilizing the experimentally observed  $a^0a^0c^-$  tilt pattern in  $\text{Sr}_2\text{CrReO}_6$  (see Section III B 2).

Yet another generic consideration is the spin-orbit coupling. We demonstrate the SOC is a relatively small perturbation in this system by comparing the Re states near the Fermi energy for the cubic reference structure computed using GGA (ie.  $U=0$ ) with and without SOC (see Fig. 2, panels c and d). As shown, the DOS only exhibits small changes upon introducing SOC. Indeed, we will demonstrate the SOC can shift the phase boundary of the COO/COD by small amounts, and this can be very relevant in the Ca-based systems (including a strong magnetization direction dependence in  $\text{Ca}_2\text{FeReO}_6$ , see Section III C).

Finally, we discuss how temperature will drive the insulator to metal transition and the structural transition associated with the COD. For the most part, we will only address ground state properties in this study, as finite temperatures will be beyond our current scope; though some of our analysis will shed light on what may occur. As outlined above, the insulating ground state in this family of materials is driven by C-type orbital ordering on the Re sites, though two main factors will influence the critical value of  $U_{\text{Re}}$ : the COD and octahedral tilting. One can imagine several different scenarios which could play out depending on the energy scales. First, the tem-

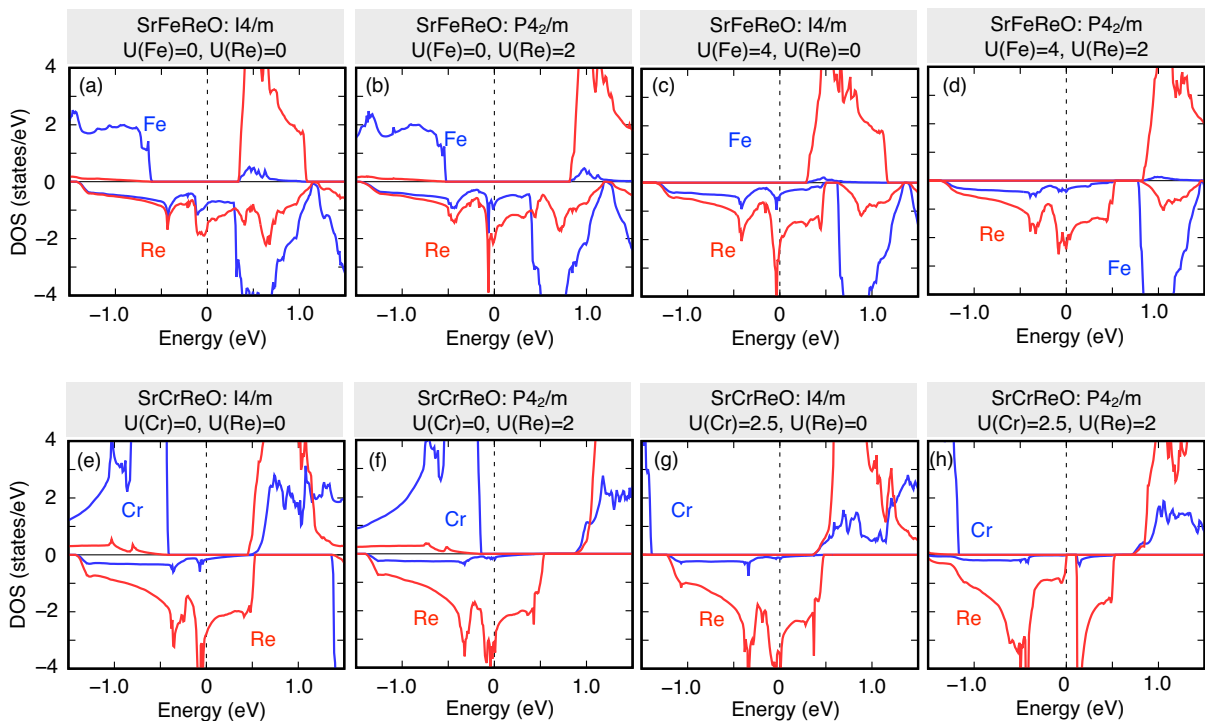


FIG. 6: Projected density of states of  $\text{Sr}_2\text{CrReO}_6$  and  $\text{Sr}_2\text{FeReO}_6$ , projected on Fe (blue), Cr (blue), and Re (red)  $d$  orbitals. Values of  $U$  and space group (obtained from relaxing internal coordinates) are indicated in each panel.

perature of the electrons could disorder the COO. Given that our DFT+ $U$  calculations predict that this COO induced insulator is Slater-like (i.e. the gap closes given ferro and other orbital orderings, see Section III B 1 and III B 2), the material will become metallic upon disordering the orbitals. Given that weak nature of the electron-phonon coupling (i.e. the COD cannot condense without an on-site  $U_{\text{Re}}$ ), this means that the COD would disorder along with the orbitals.

A different scenario can be envisioned at an opposite extreme, whereby the energy scale for orbital ordering is very large and we can neglect the electronic temperature and only consider the phonons. In this case, temperature could disorder the COD and/or the octahedral tilts which would substantially increase the critical value of  $U_{\text{Re}}$ , driving the system into a metallic state. We will entertain this latter scenario (see Section III B, and Figs. 13 in particular), though it does not appear consistent with our preferred values of  $U$  when including SOC unless there is a reorientation of the magnetization direction as seen in experiment (see Section III C, and Fig. 19). In reality, it is possible that all ingredients may be needed in order to properly capture the MIT and structural transitions from first-principles, and our paper will lay the groundwork for future study.

## B. Crystal and electronic structures

Here we compute the crystal and electronic structure of  $A_2B\text{ReO}_6$  ( $A=\text{Sr}, \text{Ca}$  and  $B=\text{Cr}, \text{Fe}$ ), exploring a range of Hubbard  $U$ s for all transition metals. We approach the four materials in order of increasing strength of electronic correlations:  $\text{Sr}_2\text{FeReO}_6$ ,  $\text{Sr}_2\text{CrReO}_6$ ,  $\text{Ca}_2\text{FeReO}_6$ ,  $\text{Ca}_2\text{CrReO}_6$ . We will address orbital ordering, axial octahedral distortions, octahedral tilt pattern, the presence of a band gap, and relative structural energetics.

### 1. $\text{Sr}_2\text{FeReO}_6$

Experimentally,  $\text{Sr}_2\text{FeReO}_6$  is found to be a metal with an  $a^0a^0c^-$  octahedral tilt pattern and  $I4/m$  symmetry (see Section I B). Given that Sr will have a smaller propensity to drive octahedral tilts relative to Ca, and that in Figure 2 we showed that Re has a larger effective bandwidth in Fe based systems as opposed to Cr based systems, it is easy to understand why  $\text{Sr}_2\text{FeReO}_6$  is the only metal among the four compounds considered.

Here we explore the interplay of octahedral tilts, octahedral distortions, and the Hubbard  $U$  in detail (see Fig. 7); including at least six different crystal structures (i.e. all structures in Fig. 5 except  $Fm\bar{3}m$  and  $P2_1/n$ ). We will use the acronym OD (i.e. octahedral distortion) to

TABLE II: Relative energy difference (in meV per formula unit) of the  $a^0a^0c^-$  structure minus the  $a^0a^0a^0$  structure for  $\text{Sr}_2\text{FeReO}_6$  within both GGA and GGA+ $U$ . The resulting space groups are indicated. We consider full structural relaxations, in addition to only relaxing internal coordinates.

$U$ (eV)	symmetry	inter. rel.	full rel.
$U_{\text{Fe}}=0, U_{\text{Re}}=0$	$I4/m - I4/mmm$	-56	-65
$U_{\text{Fe}}=4, U_{\text{Re}}=0$	$I4/m - I4/mmm$	-44	-51
$U_{\text{Fe}}=0, U_{\text{Re}}=2$	$P4_2/m - P4_2/mnm$	-55	-60
$U_{\text{Fe}}=4, U_{\text{Re}}=2$	$P4_2/m - P4_2/mnm$	-48	-53

generically refer to any spatial ordering of  $E_g^{(0)}$  octahedral distortions ( $E_g^{(0)}$  is shown schematically in Fig. 4, panels c, d and mathematically defined in Ref. [74]), such as COD for C-type ordering, FOD for ferro ordering, etc; and the same nomenclature will be used for the orbital ordering (ie. OO generically refers to COO, FOO, etc.). In the higher symmetry structures which lack an OD (i.e.  $I4/m$  and  $I4/mmm$ ), the Hubbard  $U$  may cause the electrons to spontaneously break space group symmetry despite the fact that we will prevent the nuclei from breaking symmetry; allowing us to disentangle different effects. This is achieved by using a reference crystal structure obtained from relaxing with  $U_{\text{Re}}=0$  and then retaining this structure for  $U_{\text{Re}} > 0$  (this process is repeated for different values of  $U_{\text{Fe}}/U_{\text{Cr}}$ ). Anytime a reference structure is employed, it will be indicated using an asterisk. Given that the OO/OD is a spontaneously broken symmetry for  $I4/m$ , we could have created a reference structure simply by enforcing space group symmetry, but this is not possible in the Ca-based systems where the OO/OD is not a spontaneously broken symmetry; and we prefer to have a uniform approach throughout. It should be noted that in all cases we retain the small degree of tetragonality in the lattice parameters, so there is technically always a very small tetragonal distortion ( $\sqrt{2}a=7.865$  and  $c=7.901$  [1]). Fully relaxing the lattice parameters had a very small effect on the results in the test cases we evaluated (see Table II). In all panels, solid points indicate an insulator, while hollow points indicate a metal.

It should be noted that the structures with an OO (e.g. COO, FOO, etc.) are merged into the same line for brevity, despite the fact that they have different space groups (see Fig. 5). The COO can easily be distinguished as it is always insulating in this compound (it is only favorable at larger values of  $U_{\text{Re}}$ ), and the FOO is always metallic (it is only favorable at smaller values of  $U_{\text{Re}}$ ). The same statements clearly follow for COD and FOD, given that the orbital ordering is what causes the structural distortion. Interestingly, we will show that there is a different state which can occur at intermediate values of  $U_{\text{Re}}$  in the region between the FOO/FOD and the COO/COD, and this is a ferrimagnetic orbital ordering (FIOO) and corresponding octahedral distortion

(FIOD); though the smaller magnitude OO/OD within the FIOO/FIOD is always nearly zero. These three regimes, FOO/FOD, FIOO/FIOD, and COO/COD, are easy to identify due to kinks in the curves, as we shall point out. The FIOD will prove not to be important given that it tends to lose a competition with octahedral tilting. For each structure, we present the relative energy  $\Delta E$  (ie. the energy of a reference structure with respect to the ground state, panels a and b), the band gap (panel b,c), the amplitude of the OD (denoted  $d_{|x-y|}$ , see panel d,e), and the magnitude of the OO defined as the orbital polarization (panels f and g):

$$P_{xz,yz} = \frac{1}{N_\tau} \sum_\tau \frac{|n_{d_{yz}}^\tau - n_{d_{zx}}^\tau|}{n_{d_{yz}}^\tau + n_{d_{zx}}^\tau} \quad (1)$$

where  $\tau$  labels a Re site in the unit cell, and  $N_\tau$  is the number of Re atoms in the unit cell.

We first focus on the left column of panels in Fig. 7 (i.e. a, c, e, and g), where  $U_{\text{Fe}}=4$ , though nearly qualitative behavior is independent of  $U_{\text{Fe}}$ ; the few small differences will be noted as they arise. Focussing on the blue curves corresponding to the  $*a^0a^0a^0$  structure (where the nuclei are constrained to space group  $I4/mmm$ ), we see that  $d_{|x-y|}$  is zero, as it must be when the nuclei are confined to this space group. Despite this fact,  $P_{xz,yz}$  reveals a small symmetry breaking of the electronic density for  $U_{\text{Re}} \leq 2.2$  (see panel g) where FOO is found; and this sharply transitions to a new plateau for  $2.3 \leq U_{\text{Re}} \leq 2.7$  where FIOO is found; and finally there is a sharp transition to the COO insulating state for  $U_{\text{Re}} \geq 2.8$ . Therefore, the MIT occurs at approximately  $U_{\text{Re}}=2.8$  in this scenario. Inspecting the relative energy,  $\Delta E$  is roughly constant up until approximately  $U_{\text{Re}}=2$ , whereafter  $\Delta E$  increases linearly due to the fact that the ground state structure has formed the COO/COD.

Allowing the COD to condense, but still in the absence of tilts, will shift the orbital ordering to lower values of  $U_{\text{Re}}$ ; and this is illustrated in the red curves labeled  $a^0a^0a^0+\text{OD}$  (space group  $Fmmm$  and  $P4_2/mnm$  for the FOD and COD, respectively). A jump in the value of the OD amplitude  $d_{|x-y|}$  can be seen occurring concomitantly with the orbital polarization. Clearly, the COD cooperates with the COO, allowing the latter to form at smaller values of  $U_{\text{Re}}$  and saturate at larger values. Here  $\Delta E$  has two clear kinks in the slope, given that the curve begins as roughly constant, then changes to linear when the ground state forms the COO/COD, and then becomes constant once again when the COO/COD forms in this  $a^0a^0a^0+\text{OD}$  structure.

We can now explore the results where we allow  $a^0a^0c^-$  tilts, but not the OD (ie. nuclei are frozen in  $I4/m$  space group, see green curves labeled  $*a^0a^0c^-$ ). The tilts also reduce the threshold  $U_{\text{Re}}$  needed to drive the COO insulating state as compared to the  $*a^0a^0a^0$  reference structure. Serendipitously, this reduction is roughly the same as the  $a^0a^0a^0+\text{OD}$  reference structure; though we see that when comparing the energetics of these two cases,

TABLE III: Magnetic moment  $M$  ( $\mu_B$ ) and  $N_d$  of Cr/Fe and Re atoms in Re-DPs within GGA and GGA+ $U$ , where  $U_{\text{Cr}}=2.5$ ,  $U_{\text{Fe}}=4$ , and  $U_{\text{Re}}=2$ .

	$M(\text{Cr/Fe})$		$M(\text{Re})$	
	GGA	GGA+ $U$	GGA	GGA+ $U$
$\text{Sr}_2\text{FeReO}_6$	3.647	4.086	0.815	1.340
$\text{Sr}_2\text{CrReO}_6$	2.239	2.647	1.068	1.532
$\text{Ca}_2\text{FeReO}_6$	3.593	4.094	0.804	1.411
$\text{Ca}_2\text{CrReO}_6$	2.329	2.689	1.135	1.581

	$N_d(\text{Cr/Fe})$		$N_d(\text{Re})$	
	GGA	GGA+ $U$	GGA	GGA+ $U$
$\text{Sr}_2\text{FeReO}_6$	5.896	5.743	4.178	4.140
$\text{Sr}_2\text{CrReO}_6$	4.131	4.075	4.251	4.210
$\text{Ca}_2\text{FeReO}_6$	5.884	5.717	4.171	4.152
$\text{Ca}_2\text{CrReO}_6$	4.107	4.031	4.229	4.194

$*a^0a^0c^-$  is favorable up to the largest  $U_{\text{Re}}$  considered (see panel a). It should be noted that the ferri FIOO state is not realized in this case (ie. FOO transitions directly to COO).

Finally, we can allow both  $a^0a^0c^-$  tilts and the OD (ie. space group  $P4_2/m$ , see black curves labeled  $a^0a^0c^-+OD$ ), which cooperate to strongly reduce the threshold for the COO insulating state to  $U_{\text{Re}}=2.1$ . Interestingly, this appears to occur because the tilts have a preference for converting the FIOD to the COD (see panels e and g), which appears reasonable given that the tilt pattern of the Re alternates in the z-direction with the same phase as the COD. All of the same generic trends can be observed in the right column where  $U_{\text{Fe}}=0$ , though all transitions are shifted to higher values of  $U_{\text{Re}}$  as is expected for a larger effective Re bandwidth.

Given that  $\text{Sr}_2\text{FeReO}_6$  is metallic in experiment, and that we expect  $U_{\text{Fe}}=4$  to be a reasonable value, we would infer that  $U_{\text{Re}} \leq 2.0$  in order to be consistent with experiment (see Section IIID for a more detailed discussion). In the region  $U_{\text{Re}} \leq 2.0$ , the energy differences are nearly constant, and it is worth noting that the predicted energy gain for octahedral tilting is reasonable given the experimentally observed transition from  $I4/m \rightarrow Fm\bar{3}m$  at  $T = 490\text{K}$ .

It is also useful to determine the effect of  $U$  on the magnetic moment of the transition metal sites in addition to the number of electrons ( $N_d$ ) in the correlated manifold (see Table III). The Fe and Re moments are 3.65 (4.09) and 0.82 (1.34)  $\mu_B$ , respectively, within GGA (GGA+ $U$ ). The number of  $d$  electrons decreases by roughly 0.15 electrons for Fe as  $U$  is turned on, reflecting the unmixing the Fe; while the changes in Re are more modest.

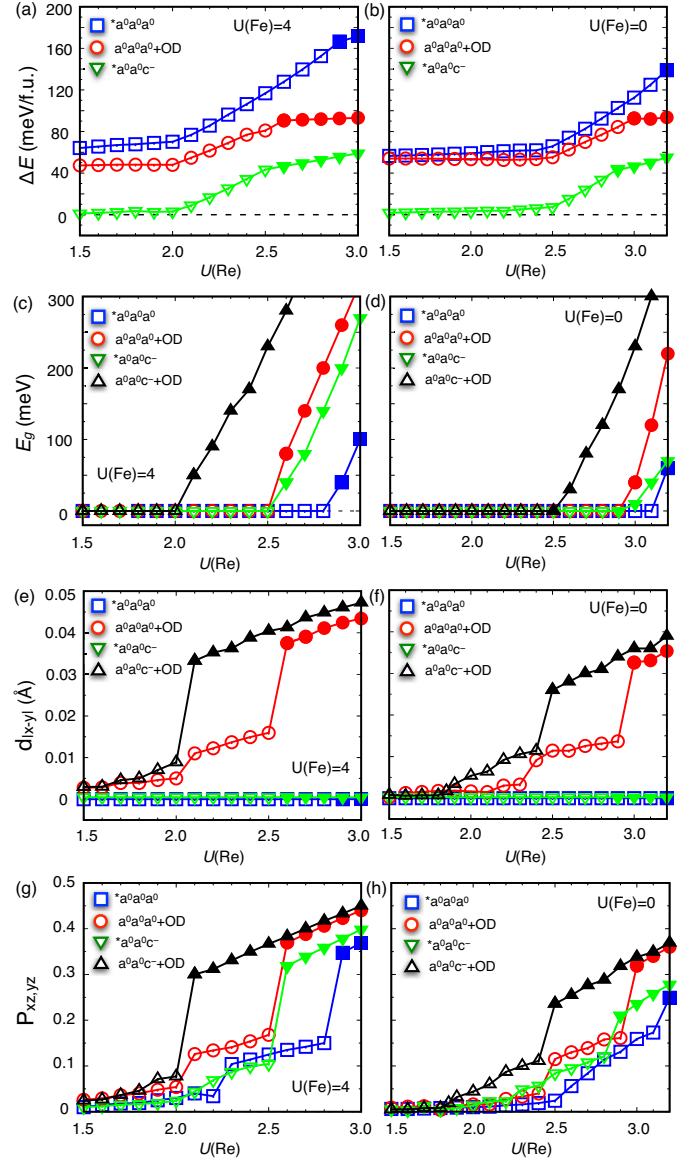


FIG. 7: (a),(b) Relative energy of  $\text{Sr}_2\text{FeReO}_6$  in several structures with respect to the ground state (ie.  $a^0a^0c^-+OD$ ). (c),(d) Electronic band gaps of different phases of  $\text{Sr}_2\text{FeReO}_6$ . (e),(f) Octahedral distortion (OD) amplitude  $d_{|x-y|}$  of the  $\text{ReO}_6$  octahedron. (g),(h) Orbital polarization  $P(d_{xz}, d_{yz})$  (see eq. 1) for Re. Panels (a), (c), (e), and (g) correspond to  $U_{\text{Fe}}=4$ , while panels (b), (d), (f), and (h) correspond to  $U_{\text{Fe}}=0$ . Filled and empty points stand for the insulating and metallic phases, respectively.

## 2. $\text{Sr}_2\text{CrReO}_6$

As we discussed in the literature review (see Section IB), several experiments suggested that  $\text{Sr}_2\text{CrReO}_6$  is metallic with space group  $I4/m$  (demanding that  $d_{|x-y|}=0$ )[1, 2, 25, 26]. However, recently Hauser *et al.* proposed that a fully-ordered  $\text{Sr}_2\text{CrReO}_6$  film on the

STO substrate is in fact a semiconductor with  $E_{\text{gap}}=0.21$  eV [3], and further suggested that the previously reported half-metallicity of  $\text{Sr}_2\text{CrReO}_6$  may be due to oxygen vacancies [23]. Our calculations lend support to the observations of Hauser *et al.*, showing that the COO/COD can induce an insulating state for reasonable values of  $U_{\text{Re}}$ .

Here we perform the same analysis for  $\text{Sr}_2\text{CrReO}_6$  as in the previous section for  $\text{Sr}_2\text{FeReO}_6$ , demonstrating the same generic behavior; but different quantitative thresholds (see Fig. 8). The main notable difference observed in  $\text{Sr}_2\text{CrReO}_6$  as compared to  $\text{Sr}_2\text{FeReO}_6$  is the energy scale for octahedral tilting, where  $U_{\text{Cr}}$  plays a role in stabilizing the tilt pattern. For example, when  $U_{\text{Cr}}=0$  octahedral tilting is either unstable or stabilized by less than 1meV, depending on whether or not one relaxes lattice parameters in addition to internal coordinates (see Table IV). However, applying a non-zero  $U_{\text{Cr}}$  results in a small stabilization energy for  $a^0a^0c^-$  tilting, and this effect only depends weakly on  $U_{\text{Re}}$  prior to the onset of the COO (i.e.  $U_{\text{Re}} < 2$ ; see Fig. 8, panels a and b). Clearly, a non-zero  $U_{\text{Cr}}$  is essential to obtaining an energy scale for octahedral tilting which is consistent with a tilt transition of  $T = 260\text{K}$  (see Table I). Otherwise, all of the same trends from  $\text{Sr}_2\text{FeReO}_6$  can be seen in  $\text{Sr}_2\text{CrReO}_6$ . If we then take a value of  $U_{\text{Cr}}=2.5$ , an insulating state can only be achieved if  $U_{\text{Re}} \gtrsim 2$  for the ground state structure  $P4_2/m$  (i.e.  $a^0a^0c^- + \text{COD}$ ).

Given our preferred values of  $U$  (ie.  $U_{\text{Cr}}=2.5$  and  $U_{\text{Re}}=2$ ),  $\text{Sr}_2\text{CrReO}_6$  is insulating as in experiment. However, given these values of  $U$ , the COD is a necessary condition for realizing the insulating state (ie. compare the black and green curves in Fig. 8, panel c), and the COD is only energetically favorable by 5.5 meV (ie. green curve in panel a). Therefore, if thermal fluctuations of the phonons were to disorder the COD, the system would be driven through the MIT. The system could remain insulating in the absence of the COD if  $U_{\text{Re}} \gtrsim 2.4$ , but then  $\text{Sr}_2\text{FeReO}_6$  would be insulating with a COD stabilized by 34.4 meV for  $U_{\text{Re}} = 2.4$ ; inconsistent with experiment. Therefore, the COD should condense at sufficiently low temperatures in experiment and the space group should be measured to be  $P4_2/m$  instead of  $I4/m$  given sufficiently clean samples. Later we demonstrate that SOC introduces quantitative changes, but the same general conclusion holds. Future experiments can test this prediction.

Given that the experimental insulating state was realized via growth on STO, it is worthwhile to determine the influence of imposing the STO lattice parameter ( $a=3.905$ ); which is  $\sim 0.04\%$  of compressive strain compared to the optimized lattice parameter within GGA+ $U$  (with  $U_{\text{Cr}}=2.5$  and  $U_{\text{Re}}=2$ ). We find that this strain has only a small effect on energy differences, resulting in a difference of  $-17.8$  meV for  $P4_2/m - P4_2/mnm$ , as compared to  $-18.5$  meV for the bulk case in Table IV; and therefore we do not believe the substrate has any substantial effect.

The magnetic moments and number of electrons as a

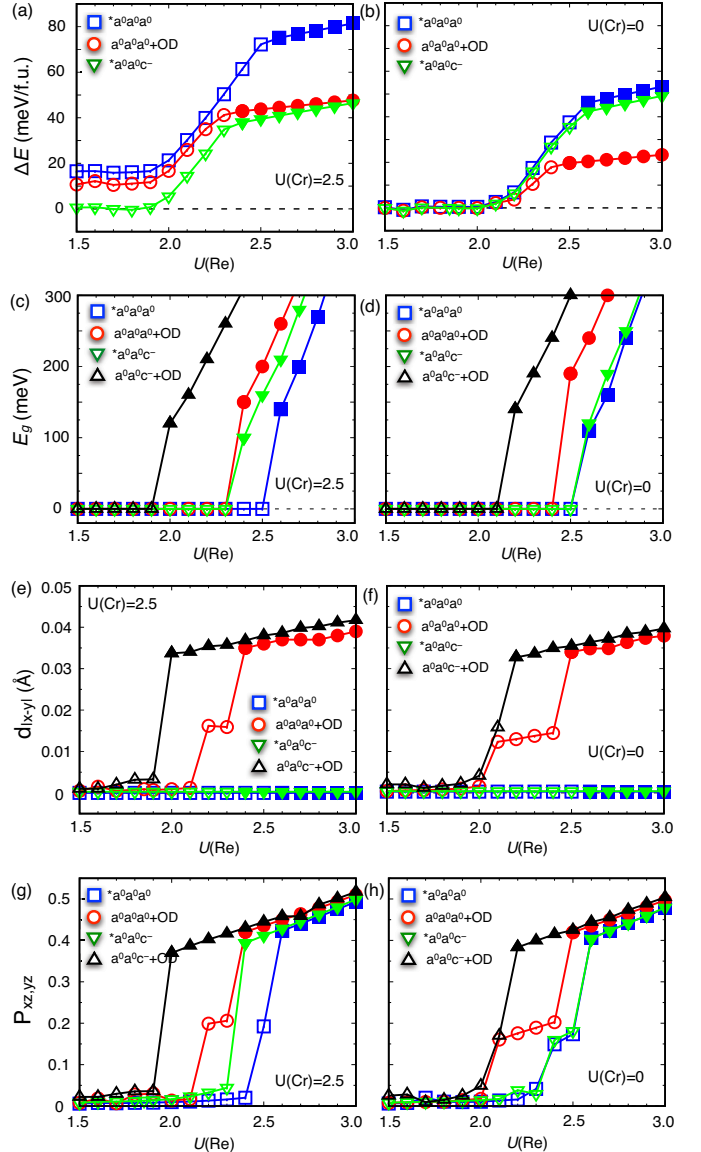


FIG. 8: (a),(b) Relative energy of  $\text{Sr}_2\text{CrReO}_6$  in several structures with respect to the ground state (ie.  $a^0a^0c^- + \text{OD}$ ). (c),(d) Electronic band gaps of different phases of  $\text{Sr}_2\text{CrReO}_6$ . (e),(f) Octahedral distortion (OD) amplitude  $d_{|x-y|}$  of the  $\text{ReO}_6$  octahedron. (g),(h) Orbital polarization  $P(d_{xz}, d_{yz})$  (see eq. 1) for Re. Panels (a), (c), (e), and (g) correspond to  $U_{\text{Cr}}=2.5$ , while panels (b), (d), (f), and (h) correspond to  $U_{\text{Cr}}=0$ . Filled and empty points stand for the insulating and metallic phases, respectively.

function of  $U$  are summarized in Table III. The Cr and Re moments are 2.24 (2.65) and 1.07 (1.53)  $\mu_B$ , respectively, within GGA (GGA+ $U$ ). However, note that the total moment is constant ( $2\mu_B/\text{f.u.}$ ) within both GGA and GGA+ $U$ . The number of d electrons decreases by  $\sim 0.06$  for Cr as  $U$  is turned on, which is almost half of the change of  $N_d$  of Fe in  $\text{Sr}_2\text{FeReO}_6$ . Smaller change of

TABLE IV: Relative energy difference (in meV per formula unit) of the  $a^0a^0c^-$  structure minus  $a^0a^0a^0$  for  $\text{Sr}_2\text{CrReO}_6$  within both the GGA and GGA+ $U$  calculations, and their crystal symmetries. We consider full structural relaxations, in addition to only relaxing internal coordinates.

$U$ (eV)	symmetry	inter. rel.	full rel.
$U_{\text{Cr}}=0, U_{\text{Re}}=0$	$I4/m - I4/mmm$	0.07	-0.06
$U_{\text{Cr}}=2.5, U_{\text{Re}}=0$	$I4/m - I4/mmm$	-4.90	-7.96
$U_{\text{Cr}}=3.5, U_{\text{Re}}=0$	$I4/m - I4/mmm$	-11.90	-13.89
$U_{\text{Cr}}=0, U_{\text{Re}}=2$	$P4_2/m - P4_2/mnm$	-0.33	-0.48
$U_{\text{Cr}}=2.5, U_{\text{Re}}=2$	$P4_2/m - P4_2/mnm$	-18.47	-20.45
$U_{\text{Cr}}=3.5, U_{\text{Re}}=2$	$P4_2/m - P4_2/mnm$	-29.67	-28.98

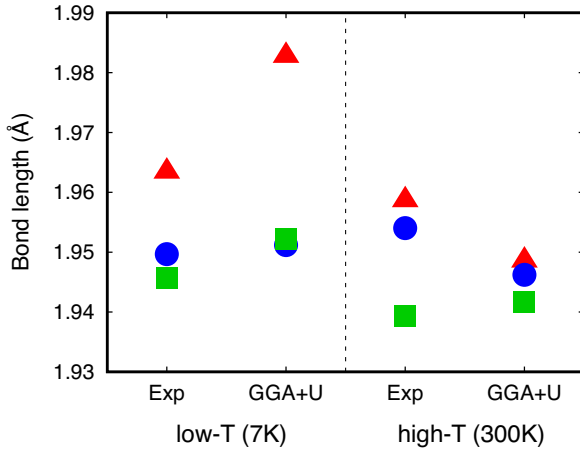


FIG. 9: Re1-O bond lengths of  $\text{Ca}_2\text{FeReO}_6$  for the experimental structures at high- and low-temperature[12], and from the relaxed structures within GGA and GGA+ $U$ . Blue circle, red triangle, and green box stand for Re1-O1, Re1-O2, and Re1-O3, respectively, where Re1-O3 is the out-of-plane Re-O bond. The Re2-O bond lengths are given by Re2-O1=Re1-O2, Re2-O2=Re1-O1, and Re2-O3=Re1-O3. Given our unit cell conventions (see Fig. 10), the experimental paper plots Re1-O in the low temperature phase and Re2-O in the high temperature phase.

$N_d(\text{Cr})$  also reflects the weaker Cr-Re hybridization.

### 3. $\text{Ca}_2\text{FeReO}_6$

We now move on to the case of  $\text{Ca}_2\text{FeReO}_6$ , which has the lower symmetry space group  $P2_1/n$  ( $a^-a^-b^+$  tilt, see Fig. 1) and is measured to be an insulator with a 50meV energy gap at low temperature (see Section IB for a detailed review). Given the smaller size of Ca relative to Sr, the tilts in both Ca-based materials are large in magnitude (see Table V for octahedral mode amplitudes) and retained up to the highest temperatures that have been studied in experiment (i.e. 300K and 550K for

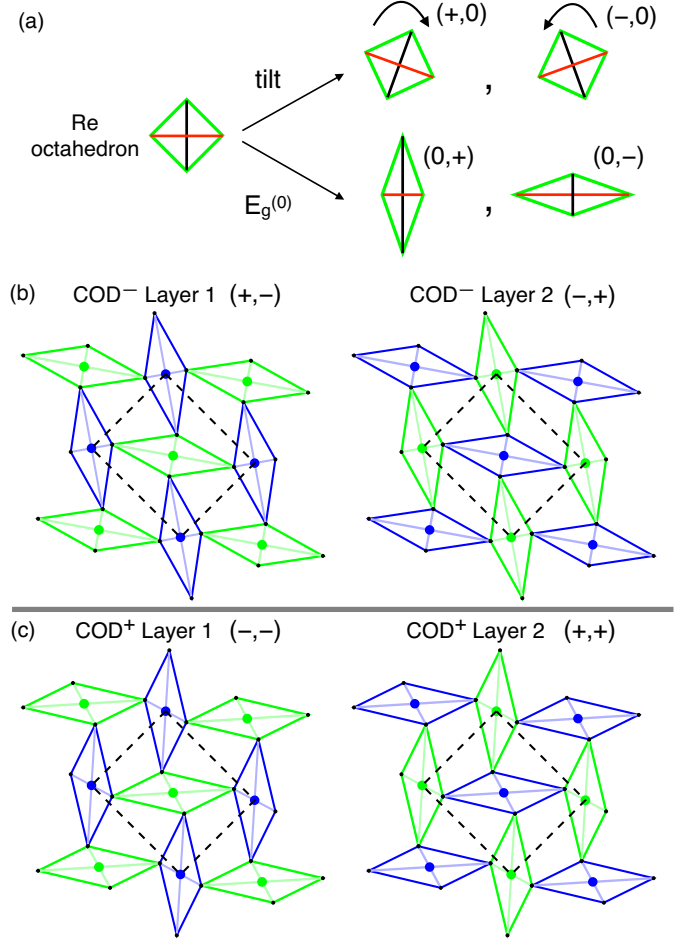


FIG. 10: (a) Signs of the tilt mode (clockwise being positive) and  $E_g^{(0)}$  mode ( $y$  elongation being positive) of Re-O octahedron. Black and red lines correspond to Re-O bonds. Quantities in parenthesis, give the sign of the tilt and  $E_g^{(0)}$  amplitude, respectively. (b), (c) Two dimensional schematic of the two possible orientations of COD: COD<sup>-</sup> and COD<sup>+</sup>. Black dots represent oxygen, green dots represent Re, and blue dots represent  $B$  atom (Fe or Cr). The dashed rectangle is the unit cell, where  $a < b$ . The coordinate system is the same as depicted in Fig. 4. Each schematic is defined by three numbers: the tetragonality of the unit cell, the octahedral tilt amplitude, and the amplitude of the  $E_g^{(0)}$  mode. Panels (a) and (b) (i.e. COD<sup>-</sup> and COD<sup>+</sup>, respectively) only differ in the sign of the octahedral tilt amplitude. The amplitudes of the distortions are exaggerated to showcase the difference between COD<sup>+</sup> and COD<sup>-</sup>.

$\text{Ca}_2\text{CrReO}_6$  and  $\text{Ca}_2\text{FeReO}_6$ , respectively). For example, two in-plane and one out-of-plane  $\angle\text{Fe-O-Re}$  are 151.2, 151.8, and 152.4° at 7K, and both DFT and DFT+ $U$  accurately capture the large magnitude of the octahedral tilts:  $\angle\text{Fe-O-Re}$  are 149.9, 151.1, 150.5 using DFT; 149.7, 150.0, and 150.8° using DFT+ $U$  ( $U_{\text{Fe}}=4$  and  $U_{\text{Re}}=2$ ). Furthermore, these large tilts substantially reduce the effective Re bandwidth, resulting in a smaller critical value of  $U_{\text{Re}}$  needed to drive the COO induced insulating state,

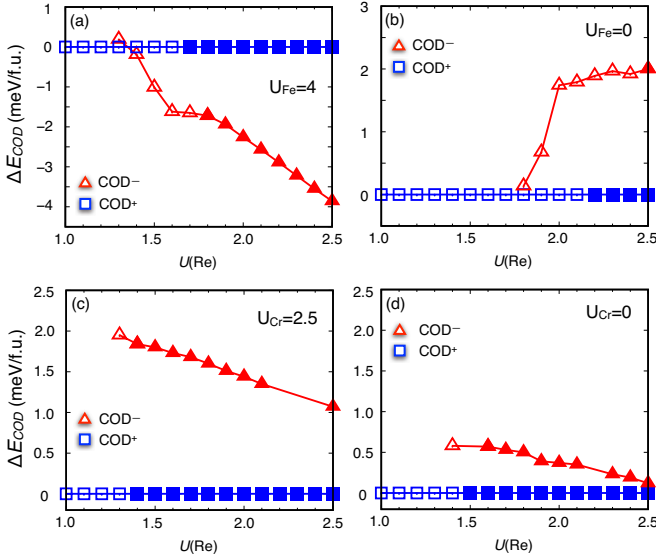


FIG. 11: Energies for  $\text{COD}^+$  (blue square) and  $\text{COD}^-$  (red triangle) relative to  $\text{COD}^+$  as a function of  $U_{\text{Re}}$ . (a),(b)  $\text{Ca}_2\text{FeReO}_6$  with  $U_{\text{Fe}}=4$  and  $U_{\text{Fe}}=0$ , respectively. (c),(d)  $\text{Ca}_2\text{CrReO}_6$  with  $U_{\text{Cr}}=2.5$  and  $U_{\text{Cr}}=0$ , respectively. Empty and filled points stand for metallic and insulating phases, respectively.

as we will now illustrate.

In Sec. IB, we briefly discussed the structures of  $\text{Ca}_2\text{FeReO}_6$  obtained at low and high temperatures [12], as summarized in Fig. 9. According to experiment, there is an appreciable COD amplitude below the phase transition (e.g.  $\text{COD}^+$ ,  $d_{|x-y|} = 0.014\text{\AA}$  at  $T=7\text{K}$ ), and it is highly suppressed and swapped to the alternate variant above the transition temperature of  $T = 140\text{K}$  (e.g.  $\text{COD}^-$ ,  $d_{|x-y|} = 0.005\text{\AA}$  at  $T=300\text{K}$ ). It should be emphasized that the COD is not a spontaneously broken symmetry in this structure, in contrast to the Sr case (see symmetry lineage in Fig. 5).

We now elaborate on the fact that there are two types of COD within the monoclinic  $P2_1/n$  structure (see schematic in Fig. 10). We will use a notation of  $\text{COD}^+$  to denote the ordering where a given Re-O octahedron has the same sign for the  $E_g^{(0)}$  mode (defined in the unrotated coordinate system) and the rotation mode (ie. both modes positive or both modes negative); whereas  $\text{COD}^-$  indicates opposite signs. Structures below and above the MIT exhibit  $\text{COD}^+$  and  $\text{COD}^-$ , respectively. Note that the  $\text{COD}^+$  and  $\text{COD}^-$  are distinguishable only in the monoclinic (i.e.,  $a \neq b$ ) double perovskites, whereas they are symmetry equivalent in the tetragonal double perovskites (e.g. in the Sr-based systems).

GGA results in  $\text{COD}^+$ , and  $\text{COD}^-$  is not even metastable (ie. it relaxes back to  $\text{COD}^+$ ); though the  $\text{COD}^+$  amplitude is negligibly small (i.e.,  $d_{|x-y|} < 0.001\text{\AA}$ ). The energies of  $\text{COD}^+$  and  $\text{COD}^-$  become distinct as  $U_{\text{Re}}$  increases, while the relative stability also de-

pends on  $U_{\text{Fe}}$ . As depicted in Fig. 11(a),  $\text{COD}^+$  switches to  $\text{COD}^-$  at  $U_{\text{Re}}=1.4$  when  $U_{\text{Fe}}=4$ , and the energy difference increases as a function of  $U_{\text{Re}}$ . When  $U_{\text{Fe}}=0$ , as shown in Fig. 11(b),  $\text{COD}^+$  is always favorable, and its stability increases in the range  $U_{\text{Re}}=1.8-2.5\text{eV}$ . Since the energy difference between two different orderings is very small, we simply follow  $\text{COD}^+$  (ie. low temperature orientation) whenever applying DFT+ $U$ . In terms of the COD amplitudes, GGA+ $U$  and GGA agree more closely for the low- $T$  and high- $T$  structures, respectively (see Figure 9), though GGA+ $U$  overestimates and GGA underestimates  $d_{|x-y|}$ .

We now perform the same analysis as for the Sr-based systems, except that the untilted structure does not need to be considered given its large energy scale. In the Sr-based systems, we considered high symmetry reference structures, where we allowed the electrons to spontaneously break symmetry but prevented the structure from doing so by fixing it at the relaxed  $U_{\text{Re}}=0$  structure (though non-zero  $U_{\text{Cr}}/U_{\text{Fe}}$  was included in creating a relaxed reference structure). The same recipe can be followed in the Ca-based cases, despite the fact that the  $U_{\text{Re}}=0$  structure has an identical space group symmetry, and this reference structure will be referred to as  $*a^-a^-b^+$ ; where the asterisk indicates that this a reference structure where we have effectively removed the COD which is induced by orbital ordering. Comparison to the reference structure will give insight into the importance of the COD in realizing the COO. Additionally, we will also study the unrelaxed experimentally measured structures from  $T=120\text{K}$  and  $T=160\text{K}$ , which straddle the  $T=140\text{K}$  phase transition. Due to the strong octahedral tilting, only the COO/COD is found in the Ca-based results, as opposed the Sr-based systems where ferro and ferri OO/OD's are observed.

We begin by focussing on the reference structure  $*a^-a^-b^+$ , depicted by a green curve, where the COD amplitude is negligibly small irrespective of  $U_{\text{Fe}}$  (see Fig. 12, panels e and f). Increasing  $U_{\text{Re}}$  causes the orbital polarization to increase, and an insulating state (solid point) is eventually realized at  $U_{\text{Re}}=2.4$  for the case of  $U_{\text{Fe}}=4$  (see Fig. 12, panels c, e, and g). For  $U_{\text{Fe}}=4$ , the relative energy  $\Delta E$  increases rather slowly for  $U_{\text{Re}} \lesssim 1.4$ , and the slope increases thereafter due to the fact that the ground state experiences the COO/COD at  $U_{\text{Re}} \approx 1.4$ . As in Sr-based systems, turning off the  $U$  on the  $3d$  transition metal shifts the metal-insulator phase boundary to larger values of  $U_{\text{Re}}$ , and an insulating state is not achieved for  $U_{\text{Re}} \leq 2.5$  if  $U_{\text{Fe}}=0$  (panels d, f, and h). Hereafter we focus our discussion on  $U_{\text{Fe}}=4$ , as all the same qualitative trends hold upon decreasing  $U_{\text{Fe}}$ . The experimental  $T=160\text{K}$  structure (depicted by a red curve) shows relatively small differences as compared to the  $*a^-a^-b^+$  reference structure, with the band gap being quantitatively similar.

We now move on to the fully relaxed structure, where COD amplitude is allowed to relax as  $U_{\text{Re}}$  is increased (depicted as black curve). In this discussion, we focus

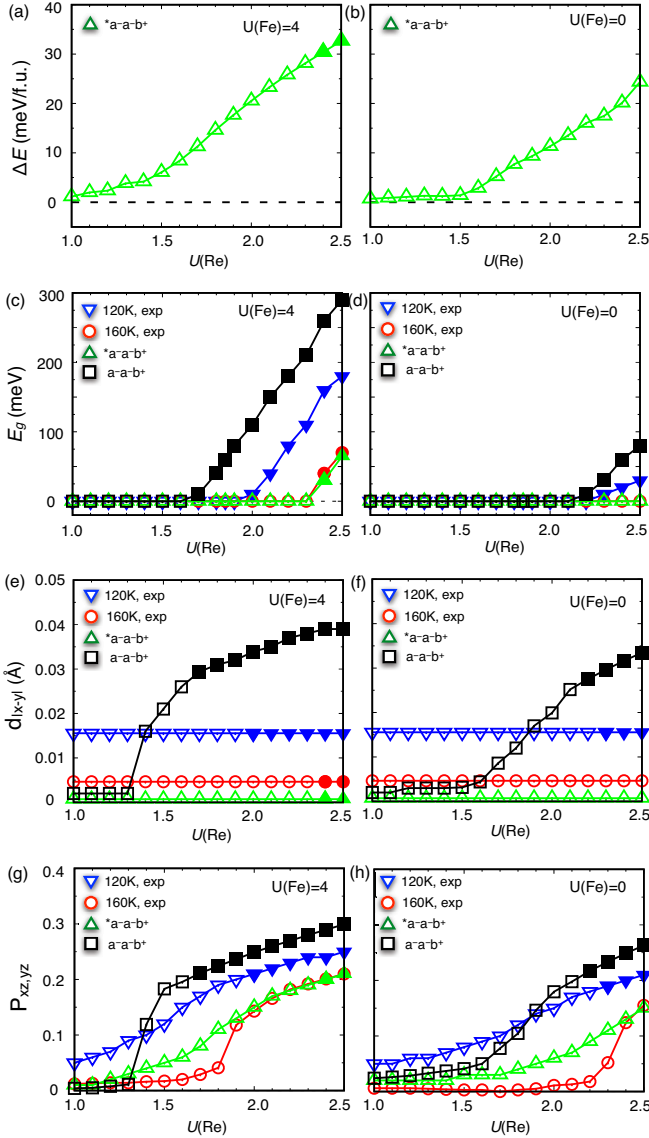


FIG. 12: (a),(b) Relative energy of  $\text{Ca}_2\text{FeReO}_6$  in the reference structure  $*a^-a^-b^+$  (where the COD amplitude is suppressed, see text) with respect to the ground state (ie.  $a^-a^-b^+$ ). (c),(d) Electronic band gaps of different phases. (e),(f) Octahedral distortion (OD) amplitude  $d_{|x-y|}$  of the  $\text{ReO}_6$  octahedron. (g),(h) Orbital polarization  $P(d_{xz}, d_{yz})$  (see eq. 1) for Re. Panels (a), (c), (e), and (g) correspond to  $U_{\text{Fe}}=4$ , while panels (b), (d), (f), and (h) correspond to  $U_{\text{Fe}}=0$ . Filled and empty points stand for the insulating and metallic phases, respectively. The frozen experimental structures at 120K and 160K[12], which bound the phase transition, are included for comparison.

on  $U_{\text{Fe}}=4$ . For  $U_{\text{Re}} \leq 1.3$ , both the orbital polarization (ie.  $P_{xz,yz}$ ) and the COD amplitude (ie.  $d_{|x-y|}$ ) are very small with a weak  $U_{\text{Re}}$  dependence; comparable in magnitude to the reference structure. Once  $U_{\text{Re}} > 1.3$ , there is a sharp increase in the COO/COD amplitude, and the system becomes an insulator for  $U_{\text{Re}} \geq 1.7$ . Therefore,

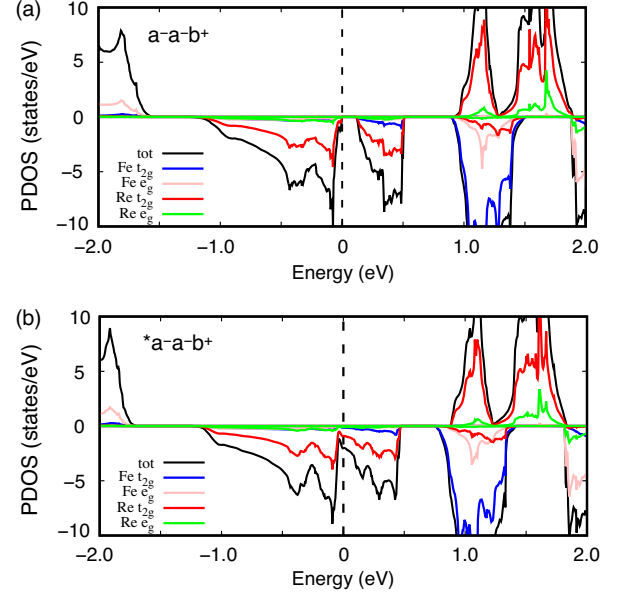


FIG. 13: DFT+U projected density of states of  $\text{Ca}_2\text{FeReO}_6$  (a) in the ground state structure ( $a^-a^-b^+$ ) (b) in the reference structure  $*a^-a^-b^+$ . The Fermi energy is set to be zero;  $U_{\text{Re}}=2.0$  and  $U_{\text{Fe}}=4$ .

the cooperation of the COO and COD greatly reduces the critical  $U_{\text{Re}}$  needed to drive the insulating state, from a value of  $U_{\text{Re}}=2.4$  in the reference  $*a^-a^-b^+$  structure down to a value of 1.7; which is the same trend as the case of the Sr-based systems. It is interesting to compare the relaxed COD amplitude to that of the  $T=120\text{K}$  experimental structure, depicted as a blue curve. In the relaxed structure, the smallest value of  $U_{\text{Re}}$  which has an insulating state is 1.7, and already the COD amplitude is nearly twice that of the experimental  $T=120\text{K}$  structure. However, later we demonstrate that including SOC dampens the COD amplitude (though not enough to agree with experiment, see Section III C, Fig. 18). The  $T=120\text{K}$  and  $T=160\text{K}$  experimental structures produce a critical  $U_{\text{Re}}$  of 2.0 and 2.4 for the COO/COD, respectively, which is still appreciably different.

Given the substantial renormalization of the critical  $U_{\text{Re}}$  between the  $*a^-a^-b^+$  reference structure and the fully relaxed structure, and analogously between the two experimental structures, it is interesting to consider the possibility of the anharmonic phonon free energy being the primary driving force of the MIT as a function of temperature. In this scenario, the structural transition is driven by the phonon free energy, and the resulting change in the structure is sufficient to renormalize the critical value of  $U_{\text{Re}}$  and drive the system through the MIT. Using our prescribed values of  $U_{\text{Re}}=2.0$  and  $U_{\text{Fe}}=4$  (given that we are not yet using spin-orbit coupling), we plot the site/orbital projected electronic density-of-states for the  $*a^-a^-b^+$  reference structure and the relaxed  $a^-a^-b^+$  structure (see Fig. 13). As shown, the

TABLE V: Nonzero octahedral modes of  $\text{ReO}_6$  in  $\text{Ca}_2\text{FeReO}_6$ , for one of the two symmetry equivalent Re atoms in the unit cell. The mathematical definition of each mode can be found in Figure 4 of Ref. [74]. The local coordinate system is chosen by having zero rotation modes (i.e., amplitude of  $T_{1g}$  modes are zero). The amplitudes for the other Re-O octahedron in the corresponding local coordinate system can be obtained by inverting the sign of  $E_g^{(0)}$ , and swapping the values of  $T_{2g}^{(1)}$  and  $T_{2g}^{(2)}$ . It should be noted that the low and high temperature experimental structures are different COD variants.

modes	exp [12]		GGA		
	7K	300K	GGA	+U	+U+SOC
$A_{1g}$	4.7834	4.7780	4.7655	4.8077	4.8146
$E_g^{(0)}$	-0.0137	-0.0046	-0.0017	-0.0335	-0.0260
$E_g^{(1)}$	-0.0126	-0.0196	-0.0066	-0.0171	-0.0012
$T_{2g}^{(0)}$	0.0005	0.0179	0.0109	0.0022	0.0078
$T_{2g}^{(1)}$	-0.0423	0.0192	-0.0293	-0.0678	-0.0582
$T_{2g}^{(2)}$	0.0225	-0.0255	0.0205	0.0256	0.0271

result is a metal for the  $*a^-a^-b^+$  structure and an insulator for the  $a^-a^-b^+$  structure, with the latter having a gap of 110meV; slightly larger than relatively small experimental gap of 50meV. While a greater value of  $U_{\text{Re}}$  would yield an insulator in the  $*a^-a^-b^+$  structure, this sort of tuning is discouraged by the fact that  $\text{Sr}_2\text{FeReO}_6$  would wrongly be driven into a COO/COD insulating state in contradiction with experiment (assuming a common value of  $U_{\text{Re}}$  is utilized). Future work will determine if this phonon driven scenario is dominant, as opposed to the other extreme where temperature disorders the electrons (see Section III A for further discussion of these scenarios).

#### 4. $\text{Ca}_2\text{CrReO}_6$

Similar to  $\text{Ca}_2\text{FeReO}_6$ ,  $\text{Ca}_2\text{CrReO}_6$  results in a monoclinic structure  $P2_1/n$  ( $a^-a^-b^+$  tilt, see Fig. 1) with an insulating ground state. Both DFT and DFT+U reasonably capture the large magnitude of the octahedral tilts: the two in-plane and one out-of-plane  $\angle\text{Cr-O-Re}$  are 153.8, 154.1, 154.9 using DFT; 151.7, 151.0 and 152.7° using DFT+U ( $U_{\text{Cr}}=2.5$  and  $U_{\text{Re}}=2$ ); and 153.1, 154.3, and 155.0° as measured at  $T=300\text{K}$  in experiment[1]. In terms of the COD amplitude, the experimental value of  $d_{|x-y|}$  at 300K reported by Kato *et al.* is 0.003 Å, which is smaller than  $d_{|x-y|} = 0.005\text{Å}$  of  $\text{Ca}_2\text{FeReO}_6$  at the same temperature[1]; and this suggests that the COD has been disordered at 300K, yet the transport still suggests an insulating state. Unfortunately, the low temperature values of  $d_{|x-y|}$  have not yet been measured, but we will demonstrate that a large COD amplitude is expected just as in the case of  $\text{Ca}_2\text{FeReO}_6$ .

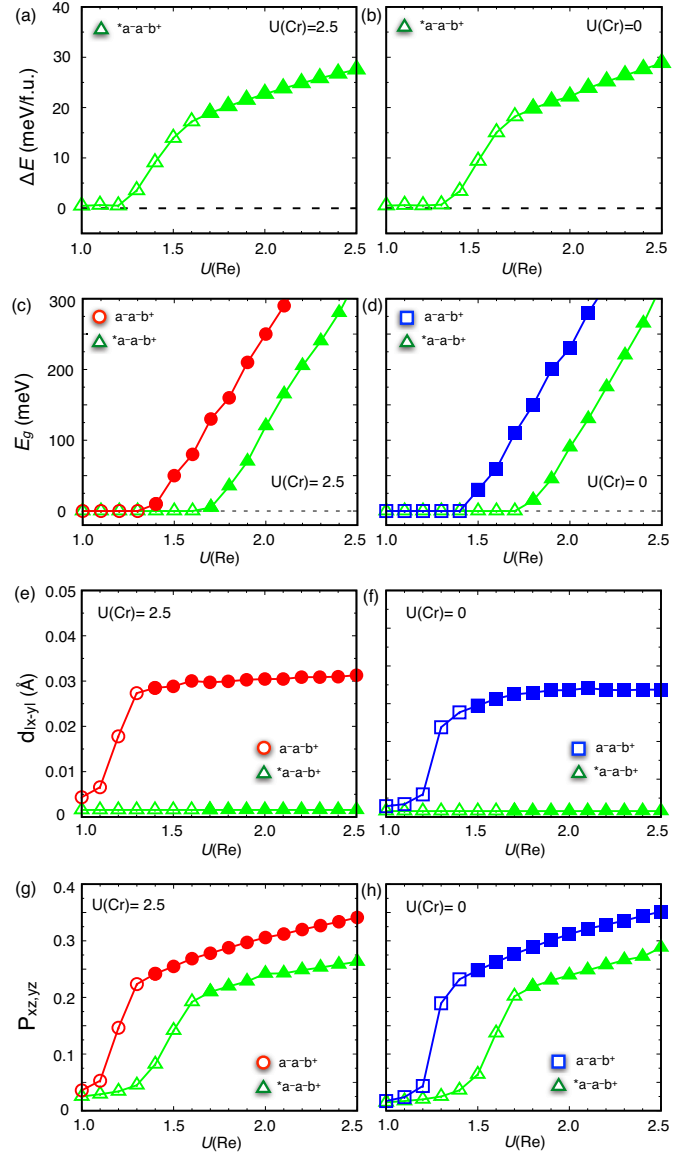


FIG. 14: (a),(b) Relative energy of  $\text{Ca}_2\text{CrReO}_6$  in the reference structure  $*a^-a^-b^+$  (where the COD amplitude is suppressed, see text) with respect to the ground state (i.e.  $a^-a^-b^+$ ). (c),(d) Electronic band gaps of different phases. (e),(f) Octahedral distortion (OD) amplitude  $d_{|x-y|}$  of the  $\text{ReO}_6$  octahedron. (g),(h) Orbital polarization  $P(d_{xz}, d_{yz})$  (see eq. 1) for Re. Panels (a), (c), (e), and (g) correspond to  $U_{\text{Cr}}=2.5$ , while panels (b), (d), (f), and (h) correspond to  $U_{\text{Cr}}=0$ . Filled and empty points stand for the insulating and metallic phases, respectively.

Just as in the case of  $\text{Ca}_2\text{FeReO}_6$ , the COD may form in either the  $\text{COD}^+$  or  $\text{COD}^-$  variant. Unlike  $\text{Ca}_2\text{FeReO}_6$ ,  $\text{COD}^+$  ordering is more stable over a broad range of  $U_{\text{Re}}$ , as depicted in Figs. 11. The energy difference between the COD variants are relatively small as compared to the case of  $\text{Ca}_2\text{FeReO}_6$ , which might be due to the smaller difference between the respective  $a$  and  $b$

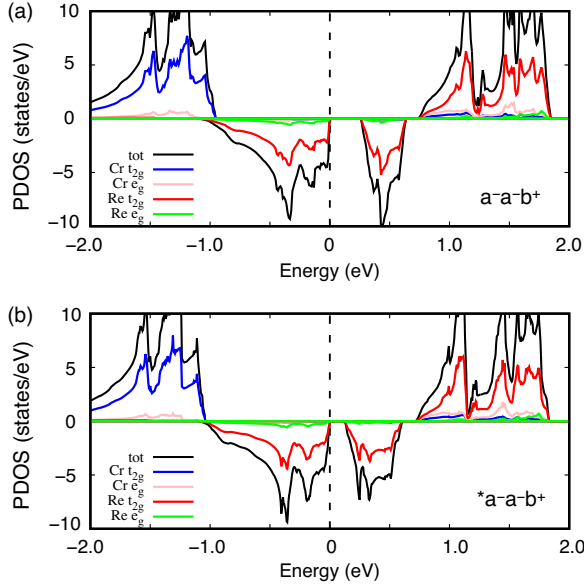


FIG. 15: DFT+ $U$  projected density of states of  $\text{Ca}_2\text{CrReO}_6$  (a) in the ground state structure ( $a^-a^-b^+$ ) (b) in the reference structure  $*a^-a^-b^+$ . The Fermi energy is set to be zero;  $U_{\text{Re}}=2.0$  and  $U_{\text{Cr}}=2.5$ .

lattice parameters. More specifically,  $b - a$  is  $0.070\text{\AA}$  in  $\text{Ca}_2\text{FeReO}_6$ , while  $b - a$  is  $0.026\text{\AA}$  in  $\text{Ca}_2\text{CrReO}_6$ . In both cases, the energy difference between  $\text{COD}^+/\text{COD}^-$  is well within the error of DFT+ $U$ . As in the case of  $\text{Ca}_2\text{FeReO}_6$ , here we only present the results of  $\text{COD}^+$  ordering.

We now perform the same analysis as in the case of  $\text{Ca}_2\text{FeReO}_6$ , computing the orbital polarization, COD amplitude, band gap, and relative energy of the ground state structure  $a^-a^-b^+$  and the reference structure  $*a^-a^-b^+$  as a function of  $U$  (see Fig. 14). The same trends are observed as compared to  $\text{Ca}_2\text{FeReO}_6$ , with the only differences being quantitative changes due to the smaller effective Re bandwidth in the Cr-based systems. Interestingly, the COD amplitude rapidly saturates after its onset, and the relative energy difference  $\Delta E$  shows three distinct regions. The third region, corresponding to  $U_{\text{Re}} > 1.6$  and  $U_{\text{Cr}}=2.5$ , corresponds to the formation of the COO in the  $*a^-a^-b^+$  reference structure, whereby the energy penalty of  $U_{\text{Re}}$  in the  $*a^-a^-b^+$  structure is reduced via polarization. This region could not be clearly seen in the  $\text{Ca}_2\text{FeReO}_6$  case given that the corresponding transition occurs just preceding the maximum value of  $U_{\text{Re}}$  in the plot, and the magnitude of the effect should be smaller given the larger effective Re bandwidth. Most importantly, the critical threshold of  $U_{\text{Re}}$  for driving the MIT is strongly reduced, requiring only  $U_{\text{Re}} = 1.4$  in the relaxed structure (with  $U_{\text{Cr}} = 2.5$ ); and a similar renormalization occurs in the reference structure  $*a^-a^-b^+$  which now only needs  $U_{\text{Re}} = 1.7$  to achieve an insulating state. This has interesting implications, as the critical  $U_{\text{Re}}$  is now sufficiently small in the reference structure

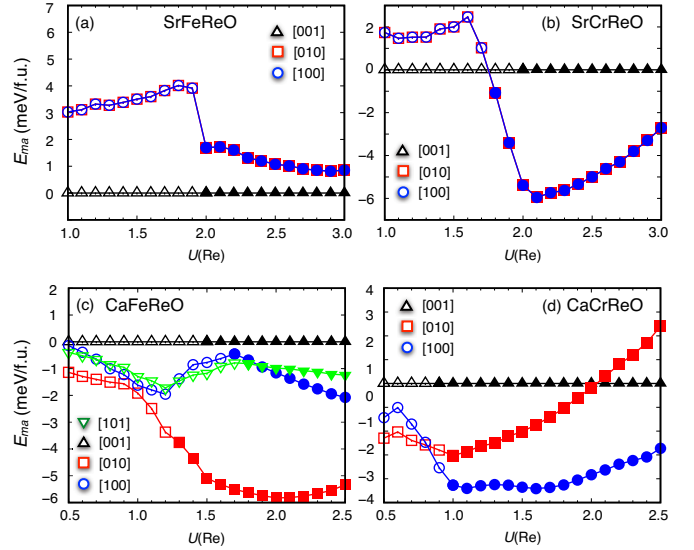


FIG. 16: Magnetic anisotropy energies as a function of  $U_{\text{Re}}$  for (a)  $\text{Sr}_2\text{FeReO}_6$ , (b)  $\text{Sr}_2\text{CrReO}_6$ , (c)  $\text{Ca}_2\text{FeReO}_6$ , and (d)  $\text{Ca}_2\text{CrReO}_6$ . Energies of the magnetization direction [001] ( $c$ -axis) is set to zero;  $U_{\text{Fe}}=4$  and  $U_{\text{Cr}}=2.5$ .

that the insulating state may survive in the absence of any appreciable COD amplitude. If we assume our preferential values of  $U_{\text{Re}} = 2$  and  $U_{\text{Cr}} = 2.5$ , we see that both the relaxed structure and the reference structure are insulators (see Fig. 15 for projected DOS). This result is consistent with the experimental measurements on  $\text{Ca}_2\text{CrReO}_6$  which find no appreciable COD amplitude, as in our reference structure, yet still measure an insulating state [1, 21]; though further experiments are clearly needed in this system before drawing conclusions.

One could argue that choosing a smaller value of  $U_{\text{Re}}$  could yield the same behavior as  $\text{Ca}_2\text{FeReO}_6$ , where the loss of the COD amplitude destroys the COO and results in a metallic state, but this sort of tuning would be forbidden by the fact that  $U_{\text{Re}} \geq 2.0$  is needed to obtain the experimentally observed insulating state in  $\text{Sr}_2\text{CrReO}_6$ . Therefore,  $\text{Ca}_2\text{CrReO}_6$  could be a concise example where orbital ordering can clearly be observed in the (near) absence of a concomitant structural distortion (ie. at a temperature where the COD is suppressed but the COO survives).

### C. Effect of spin-orbit coupling

The strength of the spin-orbit coupling ( $\lambda$ ) can be up to  $0.5\text{eV}$  in the  $5d$  transition metal oxides, which is non-negligible when compared to  $U$  and the bandwidth. In the better known example of the irridates, the  $t_{2g}$  bandwidth is approximately  $1\text{eV}$ , and thus a spin-orbit coupling of  $\lambda=0.3\text{-}0.5\text{eV}$  plays an important role in realizing the insulating state [75–77]. The effect of SOC in the Re based DPs will be smaller than the irridates given that

the  $t_{2g}$  bandwidth of Re is closer to 2eV and the strength of the SOC of Re will also be smaller due to the smaller atomic number of Re. For example, our comparison of the Re-projected DOS with and without SOC in the Sr-based systems demonstrated changes of approximately 0.2eV (see Fig. 2, panels c and d). While SOC does not qualitatively change any major trends, the small quantitative changes can be relevant; as we will demonstrate. In this section, we will explore the magnetic anisotropy energy as a function of  $U_{\text{Re}}$ , in addition to repeating our previous analysis of the orbital polarization, the OD amplitude, band gap, and relative energetics. Here we will only consider  $U_{\text{Fe}}=4$  and  $U_{\text{Cr}}=2.5$ .

We begin by considering the magnetic anisotropy energy ( $E_{ma}$ ) as summarized in Fig. 16. We define  $E_{ma}$  as the relative energy (per Re) of a given magnetic orientation with respect to the energy of the [001] orientation (e.g.  $E_{ma}[010] = E[010] - E[001]$ ). The magnetic orientation is particularly important since the threshold of  $U_{\text{Re}}$  for the COO/COD depends on the magnetic orientation, and shifts as large as 0.4eV can be observed for  $\text{Ca}_2\text{FeReO}_6$ .

For  $\text{Sr}_2\text{FeReO}_6$ , the magnetization along [001] is most stable in our calculations, as shown in Fig 16 panel (a), whereas magnetic moments are aligned in  $ab$ -plane in the experiment at 298K [78]. This appears to be a discrepancy, though we only explored [100] and [010] directions within the  $ab$ -plane, so it is possible that some other direction within the plane is lower. Also, our calculations are at  $T=0$ , while the experiments were done at  $T=298\text{K}$ . Otherwise, this could serve as an interesting failure of the method (albeit for a very small energy scale). Nonetheless,  $\text{Sr}_2\text{FeReO}_6$  is metallic with  $U_{\text{Re}} < 2.0$  in all orientations that we explored.

For  $\text{Sr}_2\text{CrReO}_6$ , the magnetization along the [100] and [010] directions are equivalent, as shown in Fig. 16 panel (b). Interestingly, [001] is more stable for small  $U_{\text{Re}}$ , but then this trend is reversed once the system goes through the COO/COD and there is a magnetic easy  $ab$  plane for  $U_{\text{Re}} \geq 1.8$ . Given our preferred values of  $U_{\text{Re}}=1.9$  and  $U_{\text{Cr}}=2.5$  (see Section III D), DFT+ $U$  results in an easy  $ab$  plane. Recent experiment by Lucy *et al.* showed that a  $\text{Sr}_2\text{CrReO}_6$  film on  $\text{SrTiO}_3$  and  $(\text{LaAlO}_3)_{0.3}(\text{Sr}_2\text{AlTaO}_6)_{0.7}$ , corresponding to 0.09% and 1.04% of compressive strains, results in a magnetic easy axis within the  $ab$  plane at both low (20K) and high  $T$  (300K) [79, 80].

For  $\text{Ca}_2\text{FeReO}_6$ , Rietveld refinement determined that the magnetization easy axis below  $T_{MIT}$  is the  $b$ -axis (ie. [010]), while above  $T_{MIT}$  the magnetization easy axis changes [12, 14]; though there is not yet consensus on the direction. Granado *et al.* suggested that Fe and Re moments lie on the  $ac$ -plane, where the magnetization angle from the  $a$  axis is  $55^\circ$  (close to [101]) [14], whereas Oikawa *et al.* showed that [001] is the easy axis [12]. We will explore [100], [010], [001], and [101] in the ground state structure, while primarily focussing on [001] in the  $*a^-a^-b^+$  reference structure; though with the latter we

investigate a few scenarios using [101].

By using the experimental atomic coordinates and LDA+ $U$  calculations ( $U_{\text{Re}}=3$  and  $J_{\text{Re}}=0.7$ ), Antonov *et al.* showed that [010] is the easy axis and [001] is lower in energy than [100], for both low  $T$  and high  $T$  experimental structures [19]. Gong *et al.* found the same result using the mBJ potential[81], despite the fact that they were using the GGA relaxed structure which more closely resembles the experimental structure above the phase transition. We also found the same ordering, which proved to be independent of the value of  $U_{\text{Re}}$ , even when crossing the COO/COD transition (see Fig. 16, panel c). Given that above the MIT Granado *et al.* found [101] to be the easy-axis, we also explore this direction; demonstrating that it is very similar to [100]. Interestingly, the magnetic orientation can have an appreciable effect on the onset of COO/COD.

For  $\text{Ca}_2\text{CrReO}_6$ , we are not aware of any experimental data on the magnetic easy axis. From an mBJ study with GGA-relaxed structure, Gong *et al.* reported that [010] is the easy axis, and  $E_{ma}[001] > E_{ma}[100]$ [81]. Alternatively, our GGA+ $U$ +SOC calculations suggest that [100] is the easy axis for  $U_{\text{Re}} \geq 0.9$  (see Fig. 16, panel (d)). Given our preferred values of  $U_{\text{Re}}=1.9$  and  $U_{\text{Cr}}=2.5$  (see Section III D), we would expect an easy axis of [100] and that [010],[001] are very close in energy.

Having established the easy axis for each material, we now repeat the previous analysis probing the behavior as a function of the Hubbard  $U$  but now including SOC and the easy axis axis as determined from DFT+ $U$  (see Figs. 17-18); and it should be kept in mind that the predicted easy-axis for  $\text{Sr}_2\text{FeReO}_6$  disagrees with experiment. Summarizing, we consider  $\text{Sr}_2\text{FeReO}_6$  [001],  $\text{Sr}_2\text{CrReO}_6$  [100],  $\text{Ca}_2\text{FeReO}_6$  [010], and  $\text{Ca}_2\text{CrReO}_6$  [100]. Given that SOC will break the block diagonal structure of the single-particle density matrix in the spin sector, it is useful to introduce a more general measure of orbital polarization rather than the definition used in equation (1); and we will utilize the standard deviation of the Eigenvalues of the local single particle density matrix for the correlated subspace, denoted  $\sigma_\tau$  (this is a component of the DFT+ $U$  energy functional, see Ref. [82] for a detailed derivation):

$$\sigma_\tau = \sqrt{\frac{\sum_m (n_m^\tau - \mu_\tau)^2}{N_{\text{orb}}}} \quad (2)$$

and

$$\mu_\tau = \frac{\sum_m n_m^\tau}{N_{\text{orb}}}, \quad (3)$$

where  $m$  labels an Eigenvalue of the single-particle density matrix for the correlated subspace (ie. Eigenvalues of the  $10 \times 10$  single-particle density matrix for the case of  $d$  electrons),  $\tau$  labels a Re site in the unit cell, and  $N_{\text{orb}}=10$  for  $d$ -electrons. The orbital polarization is then defined to be  $\sigma_\tau$ .

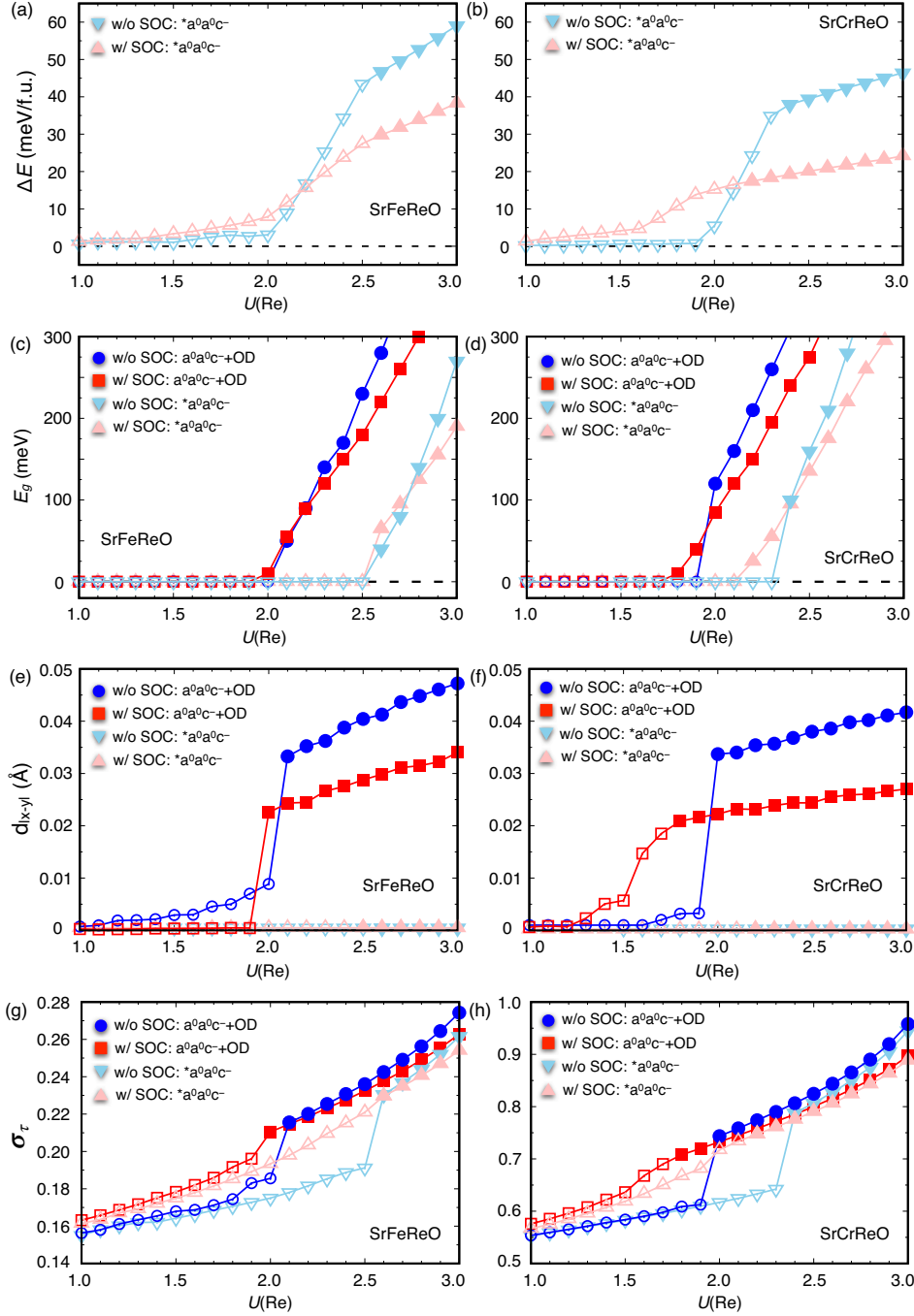


FIG. 17: (a),(b) Relative energy of Sr<sub>2</sub>FeReO<sub>6</sub> and Sr<sub>2</sub>CrReO<sub>6</sub> in the reference structure  $I4/m$  with respect to the ground state (ie.  $a^0a^0c^-$ +OD); with and without spin-orbit coupling. (c),(d) Electronic band gaps of different phases. (e),(f) Octahedral distortion (OD) amplitude  $d_{|x-y|}$  of the ReO<sub>6</sub> octahedron. (g),(h) Orbital polarization  $\sigma_\tau$  (see eq. 2) for Re. Panels (a), (c), (e), and (g) correspond to Sr<sub>2</sub>FeReO<sub>6</sub> with  $U_{\text{Fe}}=4$ , while panels (b), (d), (f), and (h) correspond to Sr<sub>2</sub>CrReO<sub>6</sub> with  $U_{\text{Cr}}=2.5$ . Filled and empty points stand for the insulating and metallic phases, respectively. Magnetization is along the [001] and [100] for Sr<sub>2</sub>FeReO<sub>6</sub> and Sr<sub>2</sub>CrReO<sub>6</sub>, respectively.

We begin with the Sr-based materials, Sr<sub>2</sub>FeReO<sub>6</sub> and Sr<sub>2</sub>CrReO<sub>6</sub>, characterizing the effect of the SOC for the relaxed structure  $a^0a^0c^-$ +OD (e.g.  $P4_2/m$  for  $a^0a^0c^-$ +COD, etc.) and the reference structure  $I4/m$  ( $*a^0a^0c^-$ ) (see Fig. 17). The previously presented results without SOC are included to facilitate comparison, in addition to providing updated values for our new metric of orbital polarization  $\sigma_\tau$ . As expected, SOC is a relatively small perturbation in all cases, though there are some interesting differences. We begin by examining the orbital polarization for the reference structures  $*a^0a^0c^-$

where the COD amplitude is restricted to be zero (see panels g and h). For smaller values of  $U_{\text{Re}}$ , prior to the COO transition, SOC enhances the orbital polarization at a given value of  $U_{\text{Re}}$  in the FOO state (comparing lines with up and down triangles). For Sr<sub>2</sub>CrReO<sub>6</sub>, the critical  $U_{\text{Re}}$  for the COO transition is shifted down by about 0.2eV (compare lines with up and down triangles), indicating the SOC is facilitating the onset of the COO and the resulting MIT. This renormalization of  $U_{\text{Re}}$  is much smaller for Sr<sub>2</sub>FeReO<sub>6</sub> and cannot be seen at the resolution we have provided. In both cases, the magnitude

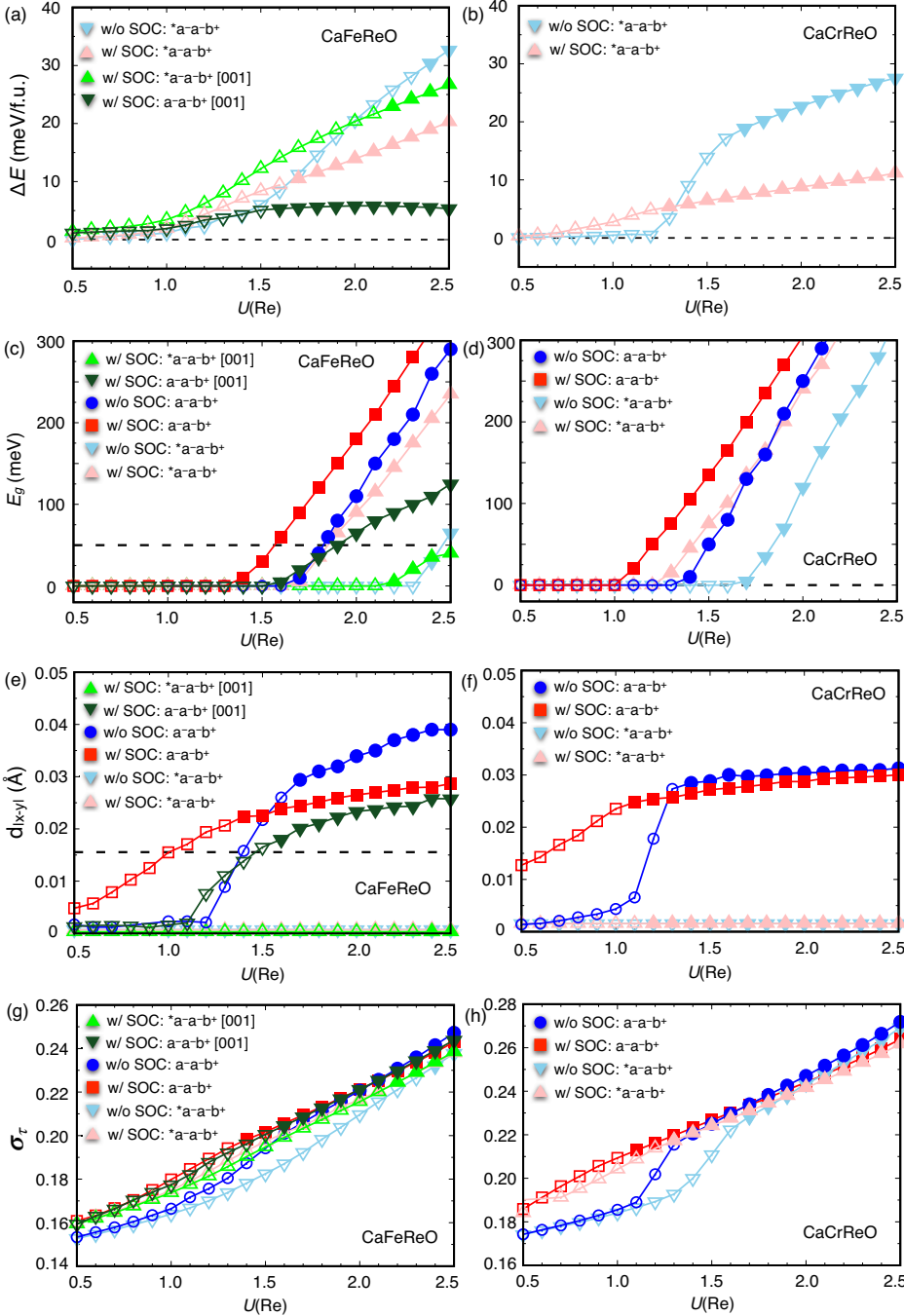


FIG. 18: (a),(b) Relative energy of Ca<sub>2</sub>FeReO<sub>6</sub> and Ca<sub>2</sub>CrReO<sub>6</sub> in the reference structure \*a<sup>-</sup>a<sup>-</sup>b<sup>+</sup> with respect to the ground state (ie. a<sup>-</sup>a<sup>-</sup>b<sup>+</sup>); with and without spin-orbit coupling. (c),(d) Electronic band gaps of different phases. (e),(f) Octahedral distortion (OD) amplitude  $d_{|x-y|}$  of the ReO<sub>6</sub> octahedron. (g),(h) Orbital polarization  $\sigma_\tau$  (see eq. 2) for Re. Panels (a), (c), (e), and (g) correspond to Ca<sub>2</sub>FeReO<sub>6</sub> with  $U_{\text{Fe}}=4$ , while panels (b), (d), (f), and (h) correspond to Ca<sub>2</sub>CrReO<sub>6</sub> with  $U_{\text{Cr}}=2.5$ . Filled and empty points stand for the insulating and metallic phases, respectively. Magnetization is along the [010] and [100] for Ca<sub>2</sub>FeReO<sub>6</sub> and Ca<sub>2</sub>CrReO<sub>6</sub>, respectively. Additionally, the [001] magnetization direction (experimentally observed for T]140K) is included for Ca<sub>2</sub>FeReO<sub>6</sub> where indicated.

of the orbital polarization beyond the COO transition is very similar with and without the SOC.

Allowing the COD to condense in the relaxed structures shows similar behavior (see red and blue curves). In both Sr<sub>2</sub>FeReO<sub>6</sub> and Sr<sub>2</sub>CrReO<sub>6</sub>, SOC pushes the onset of the COO/COD to smaller values of  $U_{\text{Re}}$ ; more substantially in the case of Cr. As a result, including SOC causes the gap to open at slightly smaller values of  $U_{\text{Re}}$ : approximately 0.1 less for Sr<sub>2</sub>FeReO<sub>6</sub> and 0.2 less for Sr<sub>2</sub>CrReO<sub>6</sub>. Notably, the COD amplitude for the metallic phase of Sr<sub>2</sub>FeReO<sub>6</sub> is dampened to zero, in agreement with experiment. Somewhat counterintuitively, SOC re-

sults in smaller COD amplitudes for values of  $U_{\text{Re}}$  beyond the MIT, despite causing an earlier onset of the COD. For the relative energetics, in both compounds SOC decreases the stabilization energy of the COD for  $U_{\text{Re}} \gtrsim 2.1$  (see panels a and b), consistent with the reduced magnitude of the COD. Given our preferred value of  $U_{\text{Re}}=1.9$  for SOC, we find that Sr<sub>2</sub>FeReO<sub>6</sub> is metallic with space group  $I4/m$  (ie. no condensation of OD), consistent with experiment; while Sr<sub>2</sub>CrReO<sub>6</sub> is insulating with a non-zero COD amplitude (ie. space group  $P4_2/m$ ), stabilized by roughly 14meV.

In the Ca-based systems, the effects of SOC are slightly

more pronounced (see Fig. 18), but the trends are all the same as the Sr-based materials. We begin by analyzing the orbital polarization in the reference structure  $*a^-a^-b^+$ , where the COD has effectively been removed (see panels g and h, curves with pink-up and blue-down triangles). For small values of  $U_{\text{Re}}$ , SOC mildly enhances the orbital polarization, but the differences diminish once both cases form the COO insulator. However, SOC has a more dramatic effect in the Ca-based systems in terms of shifting the COO induced MIT to smaller values of  $U_{\text{Re}}$ , giving a reduction of 0.7 and 0.4eV for the Fe-based and Cr-based material, respectively (see panels c and d, curves with pink-up and blue-down triangles). For the relaxed structures (see red and blue curves), the COD is activated at much smaller values of  $U_{\text{Re}}$  in both materials, more so for the case of  $\text{Ca}_2\text{CrReO}_6$ . Furthermore,  $\text{Ca}_2\text{FeReO}_6$  reaches a relatively smaller value of the COD amplitude beyond the COO induced MIT, while  $\text{Ca}_2\text{CrReO}_6$  saturates at roughly the same value. Given our preferred value of  $U_{\text{Re}}=1.9$ , both  $\text{Ca}_2\text{FeReO}_6$  and  $\text{Ca}_2\text{CrReO}_6$  are insulators with a appreciable COD amplitude, consistent with known experiments (though the low temperature structural parameters of  $\text{Ca}_2\text{CrReO}_6$  have not yet been measured). Furthermore, SOC has reduced the COD amplitude of  $\text{Ca}_2\text{FeReO}_6$ , moving it closer to the experimental value (see panel e, red curve).

For  $\text{Ca}_2\text{FeReO}_6$ , we also investigate the behavior of the [001] magnetization direction for both the reference structure  $*a^-a^-b^+$  and the ground state structure  $a^-a^-b^+$ , which is essential given that experiment dictates [001] is approximately the easy-axis above the MIT where the COD is suppressed. For  $a^-a^-b^+$ , the [001] orientation is higher in energy than [010], with the difference being enhanced as  $U_{\text{Re}}$  increases (see Fig. 16, panel c, green curve). Furthermore, for [001] the threshold value of  $U_{\text{Re}}$  for the onset of the COO/COD is increased, and the magnitude of the band gap and COD amplitude are diminished at a given value of  $U_{\text{Re}}$  (see Fig. 18, panels c and e, dark green triangles). More relevantly, the same trends are observed in the reference structure  $*a^-a^-b^+$ , but the effect is amplified (light green triangles). In particular, the critical value of  $U_{\text{Re}}$  for the COO/COD dramatically increases from 1.8 to 2.2 eV as the magnetization switches from [010] to [001] (compare pink and light green curves, respectively). We also investigate the case of [101] magnetization direction. The overall features of [101] are similar to the case of [001] (not shown), except that the critical value of  $U_{\text{Re}}$  for the COO/COD in the reference structure is increased to 2.4eV.

In Section III B 3, where SOC was not yet included, we elucidated the possibility that a suppression of the COD (e.g. via thermal fluctuations) closes the band gap via moving the critical value of  $U_{\text{Re}}$  beyond our expected value of  $U_{\text{Re}}=2.0$  within GGA+ $U$  (see Figure 13). This could have been a viable mechanism for the MIT, but SOC is strong enough to alter this scenario (see Figure 19, panels a and b, using  $U_{\text{Re}}=1.9$ ). Given the [010] magnetization direction, the gap is reduced in the reference struc-

ture, but it does not close, unlike the case where SOC is not included. However, the experiments of Oikawa *et al.* dictate that [001] should be the easy axis of the high temperature structure, in contradiction with DFT+ $U$ +SOC using our reference structure (though our predicted energy difference is less than 6meV). If we consider the [001] direction in the reference structure  $*a^-a^-b^+$ , we see that the gap has indeed closed (see Figure 19, panel (c)); the gap also closes for the [101] direction. Therefore, it is possible that the reorientation of the magnetization is important to the MIT.

In summary, we see that for  $U_{\text{Re}}=1.9$ ,  $\text{Sr}_2\text{FeReO}_6$  is a metal, while the remaining systems are COO induced insulators. The general physics that was deduced in the absence of SOC holds true with some small renormalizations of various observables. Slightly reducing the value of  $U_{\text{Re}}$  allows for results which are qualitatively consistent with experiment, with the caveat that the easy-axis of  $\text{Sr}_2\text{FeReO}_6$  disagrees with experiment.

Another interesting feature of SOC is the nonzero orbital moments of Re. Spin and orbital moments of Re within GGA+SOC and GGA+ $U$ +SOC with  $U_{\text{Re}}=1.9$  are summarized in Table VI. The direction of Re orbital moment is opposite to the spin moment, in agreement with the previous experiments [20, 83, 84] and GGA+SOC [85, 86].

As presented in Table VI, varying results have been measured for the magnitude of spin and orbital moments by different groups. However, the  $|m_L/m_S|$  values are more or less consistent [20, 83] since this quantity is not affected by possible uncertainties in the calculated number of holes [20], thus these values are better quantities to compare theory and experiments. While GGA largely underestimate the experimental  $|m_L/m_S|$  values, GGA+ $U$  gives a much better estimation for  $|m_L/m_S|$ .

#### D. Optimal $U$ values

Exploring a range of  $U$  is a necessary burden for several reasons. First, the procedure for constructing both the interactions and the double-counting correction is still an open problem. Second, given that the DFT+ $U$  method is equivalent to DFT+DMFT when the DMFT impurity problem is solved within Hartree-Fock[88], DFT+ $U$  contains well known errors which may be partially compensated by artificially renormalizing the  $U$  to smaller values. Given that our most basic concern in this paper is to develop a qualitative, and perhaps even semi-quantitative, understanding of an entire family of Re-based double perovskites, performing an empirical search for a single set of  $U$ 's which can capture the physics of this family was essential.

In Sec III B and III C, we have explored various observables for a range of values of  $U$ . Clearly,  $U_{\text{Re}}$  is the main influence, as it is a necessary condition for driving the COO insulating state in the entire family of materials, in addition to the COD. However, we also demonstrated

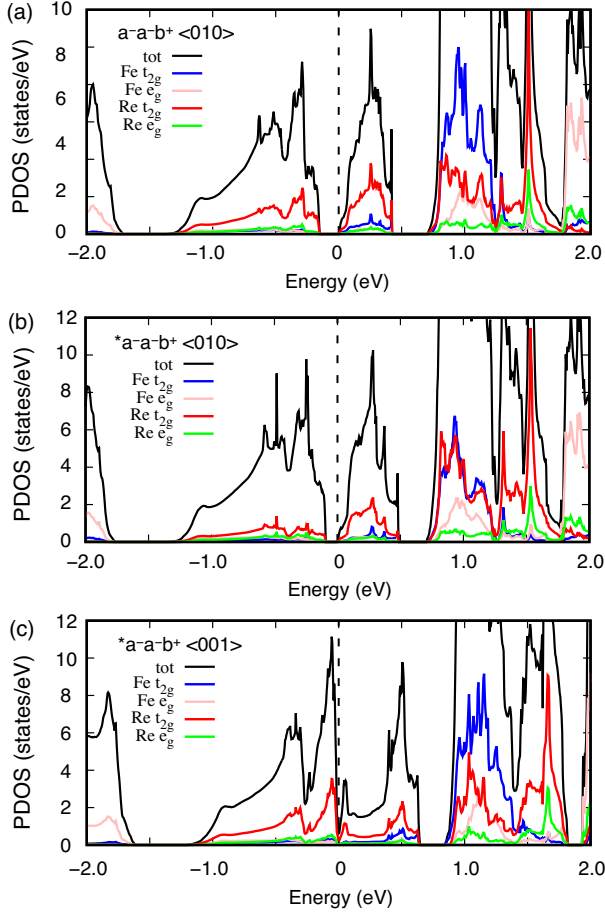


FIG. 19: DFT+ $U$ +SOC projected density of states of  $\text{Ca}_2\text{FeReO}_6$  (a) in the ground state structure ( $a^- a^- b^+$ ) with the  $[010]$  magnetization direction, (b) in the reference structure ( $*a^- a^- b^+$ ) with the  $[010]$  magnetization direction, (c) in the reference structure ( $*a^- a^- b^+$ ) with the  $[001]$  magnetization direction. The Fermi energy is set to be zero;  $U_{\text{Re}}=1.9$  and  $U_{\text{Fe}}=4$ .

that the  $U$  of the  $3d$  transition metal could play an important indirect role, via renormalizing the critical value of  $U_{\text{Re}}$  for the COO/COD to smaller values. Also, for the case of  $\text{Sr}_2\text{CrReO}_6$ , a nonzero  $U_{\text{Cr}}$  was important for properly capturing the energetics of the  $a^0 a^0 c^-$  tilt pattern. For the  $3d$  transition metals, we typically only explored  $U=0$  and another value which is in line with expectations based on previous literature or methods for computing  $U$ . For Cr, we used  $U_{\text{Cr}}=2.5$  eV, which is similar to values used for  $\text{CaCrO}_3$  [89] and Cr-related DPs ( $U=3$  eV and  $J=0.87$  eV) [85]. For Fe, we focus on  $U_{\text{Fe}}=4$  eV, as widely used elsewhere [16, 18, 85]. Excessive tuning of  $U_{\text{Fe}}$  or  $U_{\text{Cr}}$  is not needed based on our results, and the nonzero values that we evaluated were either necessary to capture a given phenomena (ie. the tilts in  $\text{Sr}_2\text{CrReO}_6$ ), or were needed for a consistent and reasonable value of  $U_{\text{Re}}$  (via the indirect influence of the  $U_{\text{Fe}}$  or  $U_{\text{Cr}}$ ). Therefore,  $U_{\text{Fe}}=4$  eV and  $U_{\text{Cr}}=2.5$  eV are rea-

TABLE VI: Spin ( $m_S$ ), orbital ( $m_L$ ), and total ( $M_{\text{tot}}$ ) moments of Re in DPs. Values are given in  $\mu_B/\text{Re}$ .

	$m_S$	$m_L$	$M_{\text{tot}}$	$ m_L/m_S $	method
$\text{Sr}_2\text{FeReO}_6$	-0.74	0.21	-0.53	0.28	exp [20]
	-1.07	0.33	-0.74	0.31	exp [83]
	-0.85	0.23	-0.62	0.27	GGA [85]
	-0.68	0.15	-0.53	0.22	GGA [20]
	-0.73	0.18	-0.55	0.25	LDA [19]
	-0.88	0.24	-0.64	0.28	LDA+ $U$ [19]
	-1.01	0.26	-0.75	0.26	mBJ [87]
	-0.76	0.16	-0.61	0.20	GGA
	-1.22	0.42	-0.83	0.34	GGA+ $U$
$\text{Sr}_2\text{CrReO}_6$	-0.68	0.25	-0.43	0.37	exp [25]
	-0.85	0.18	-0.67	0.21	GGA [86]
	-1.17	0.31	-0.85	0.27	mBJ [87]
	-0.99	0.19	-0.80	0.19	GGA
	-1.40	0.48	-0.95	0.35	GGA+ $U$
	$\text{Ca}_2\text{FeReO}_6$	-0.47	0.16	-0.31	0.34
-1.15		0.39	-0.76	0.34	exp [83]
-0.75		0.34	-0.42	0.45	LDA [19]
-1.11		0.66	-0.45	0.60	LDA+ $U$ [19]
-1.10		0.18	-0.91	0.17	mBJ [81]
-0.76		0.17	-0.58	0.23	GGA
-1.30		0.43	-0.87	0.33	GGA+ $U$
$\text{Ca}_2\text{CrReO}_6$	-1.24	0.19	-1.05	0.15	mBJ [81]
	-1.04	0.24	-0.80	0.23	GGA
	-1.41	0.56	-0.85	0.40	GGA+ $U$

sonable values to adopt, though a range of values could likely give sufficient behavior.

In the case of  $U_{\text{Re}}$ , we explored a large number of values between 0-3.2eV. The overall goal for selecting a set of  $U$ 's is to obtain the proper ground states in the entire family of materials, which is nontrivial given that  $\text{Sr}_2\text{FeReO}_6$  is metallic and the rest are insulators. While it is possible for  $U_{\text{Re}}$  to have small changes due to differences in screening among the four materials, these differences should be relatively small given the localized nature of the  $d$  orbitals which comprise the correlated subspace; and therefore we do seek a common value for all four compounds. We conclude that  $U_{\text{Re}}=2.0$  and  $1.9$  are reasonable values within GGA+ $U$  and GGA+ $U$ +SOC, respectively, and these values will properly result in a metal for  $\text{Sr}_2\text{FeReO}_6$  and insulators for the rest. The predicted bandgap  $E_{\text{gap}}$  for  $\text{Ca}_2\text{FeReO}_6$  (i.e. 105meV and 150meV within GGA+ $U$  and GGA+ $U$ +SOC, respectively) is somewhat larger than the experiment (i.e. 50meV), but this seems reasonable given the nature of approximations we are dealing with. For  $\text{Ca}_2\text{CrReO}_6$ , we obtain  $E_{\text{gap}}=250$  and 270meV using GGA+ $U$  and GGA+ $U$ +SOC, respectively (experimental gap is not known); while  $E_{\text{gap}}$  of  $\text{Sr}_2\text{CrReO}_6$  within GGA+ $U$  and GGA+ $U$ +SOC is 120 and 40meV, respectively, some-

what smaller than the experimental value of 200meV [3].

It is also interesting to compute  $U_{\text{Re}}$  via the linear response approach [90]. In  $\text{Sr}_2\text{CrReO}_6$  and  $\text{Ca}_2\text{CrReO}_6$ , we obtained  $U_{\text{Re}}=1.3$  for both systems; the calculation employed a supercell containing 8 Re atoms. Therefore, linear response predicts a relatively small value for  $U$ , consistent with  $5d$  electrons, but too small in order to be qualitatively correct:  $\text{Sr}_2\text{CrReO}_6$  could not be an insulator with such a small value.

#### IV. Summary

In summary, we investigate the electronic and structural properties of Re-based double perovskites  $A_2B\text{ReO}_6$  ( $A=\text{Sr}, \text{Ca}$  and  $B=\text{Cr}, \text{Fe}$ ) through density-functional theory +  $U$  calculations, with and without spin-orbit coupling. All four compounds share a common low energy Hamiltonian, which is a relatively narrow Re  $t_{2g}$  minority spin band that results from strong antiferromagnetic coupling to filled  $3d$  majority spin shell (or sub-shell) of the  $B$  ion. Cr results in a narrower Re  $t_{2g}$  bandwidth than Fe, while Ca-induced tilts result in a narrower Re  $t_{2g}$  bandwidth than Sr-induced tilts; resulting in a ranking of the Re  $t_{2g}$  bandwidth as  $\text{Sr}_2\text{FeReO}_6$ ,  $\text{Sr}_2\text{CrReO}_6$ ,  $\text{Ca}_2\text{FeReO}_6$ , and  $\text{Ca}_2\text{CrReO}_6$  (from largest to smallest). Spin orbit coupling is demonstrated to be a relatively small perturbation, though it still can result in relevant quantitative changes.

In general, we show that the on-site  $U_{\text{Re}}$  drives a C-type (i.e.  $\vec{q} = (0, \frac{1}{2}, \frac{1}{2})$ ) given the primitive face-centered cubic unit cell of the double perovskite) antiferro orbital ordering (denoted COO) of the Re  $d_{xz}/d_{yz}$  minority spin orbitals, along with minority  $d_{xy}$  being filled on each site, resulting in an insulating ground state. This generic phenomena can even occur in a cubic reference structure ( $Fm\bar{3}m$ ) in the absence of any structural distortions for reasonable values of  $U_{\text{Re}}$ . Furthermore, allowing structural distortions demonstrates that this C-type orbital ordering is accompanied by a local  $E_g$  structural distortion of the octahedra with C-type ordering (denoted as COD); and it should be emphasized that  $U_{\text{Re}}$  is a necessary condition for the COO/COD to occur. The COO/COD will be a spontaneously broken symmetry for  $a^0a^0c^-$ -type tilt patterns as in the Sr based systems (i.e.  $I4/m \rightarrow P4_2/m$ ), whereas not for the  $a^-a^-b^+$ -type tilting pattern of the Ca based systems (i.e.  $P2_1/n \rightarrow P2_1/n$ ).

While  $U_{\text{Re}}$  is a necessary condition for obtaining an insulating state, the presence of the COD will reduce the critical value of  $U_{\text{Re}}$  necessary for driving the orbitally ordered insulating state; as will the  $U$  on the  $3d$  transition metal. Furthermore, the COD is necessary for reducing the critical  $U_{\text{Re}}$  to a sufficiently small value such that  $\text{Sr}_2\text{FeReO}_6$  remains metallic while  $\text{Sr}_2\text{CrReO}_6$  is insulating. More specifically, using a single set of interaction parameters (i.e.  $U_{\text{Re}} = 1.9eV$ ,  $U_{\text{Fe}} = 4eV$ ,  $U_{\text{Cr}} = 2.5eV$ , when using SOC), we show that  $\text{Sr}_2\text{CrReO}_6$ ,

$\text{Ca}_2\text{CrReO}_6$ , and  $\text{Ca}_2\text{FeReO}_6$  are all insulators, while  $\text{Sr}_2\text{FeReO}_6$  is a metal; consistent with most recent experiments.

Previous experiments concluded that  $\text{Sr}_2\text{CrReO}_6$  was half-metallic [1, 2, 20–22], but recent experiments showed that fully ordered films grown on an STO substrate are insulating[3, 23]. We show that  $\text{Sr}_2\text{CrReO}_6$  is indeed insulating with  $U_{\text{Re}} = 1.9eV$ , so long as the structure is allowed to relax and condense the COD. Given that the COD is a spontaneously broken symmetry in this case, the challenge for experimental verification will be resolving the  $P4_2/m$  space group at low temperatures instead of the higher symmetry  $I4/m$  group.

While the COD is not a spontaneously broken symmetry in  $\text{Ca}_2\text{FeReO}_6$ , experiment dictates that there is an unusual discontinuous phase transition at  $T=140\text{K}$  between two structures with the same space group,  $P2_1/n$ ; with the high temperature structure being metallic and the low temperature structure being insulating. The main structural difference between the experimental structures is the COD amplitude:  $d_{|x-y|}$  is 0.016 and 0.005Å in the structures at 120K and 160K, respectively. Additionally, the COD changes variants across the transition, going from  $\text{COD}^+$  (120K) to  $\text{COD}^-$  (160K). The appreciable  $\text{COD}^+$  amplitude measured in low temperature experiments is consistent with our prediction of a large COD amplitude which is induced by the COO. The same trends are found in  $\text{Ca}_2\text{CrReO}_6$ , which has a narrower Re bandwidth and results in a more robust insulator with a larger band gap. Predicting the transition temperature from first-principles will be a great future challenge given that the temperature of the electrons and the phonons may need to be treated on the same footing, all while accounting for the spin-orbit coupling.

SOC is a small quantitative effect, though it can have relevant impact, such as lowering the threshold value of  $U_{\text{Re}}$  for inducing the COO/COD in the Ca-based compounds; even having a strong dependence on magnetization direction for  $\text{Ca}_2\text{FeReO}_6$ . GGA+ $U$ +SOC predicts the easy axis of  $\text{Sr}_2\text{CrReO}_6$  and  $\text{Ca}_2\text{FeReO}_6$  to be  $\{100\}$  and  $[010]$ , respectively, consistent with the experiment, and also compares well to the experimental measurements of the magnitude of the orbital moment. It should be emphasized that  $U_{\text{Re}}$ , and the COO/COD which it induces, is critical to obtaining the qualitatively correct easy-axis in  $\text{Sr}_2\text{CrReO}_6$ . In the case  $\text{Sr}_2\text{FeReO}_6$ , GGA+ $U$ +SOC predicts a  $[001]$  easy axis, in disagreement with one experiment which measured the easy axis to be in the  $a-b$  plane. Additionally, the GGA+ $U$ +SOC predicted ratios of orbital/spin moment  $m_L/m_s$  are close to the experimental values, whereas GGA+SOC largely underestimates them.

#### V. Acknowledgments

We thank to K. Oikawa and K. Park for helpful discussion. This work was supported by the grant de-sc0016507

funded by the U.S. Department of Energy, Office of Science. This research used resources of the National Energy Research Scientific Computing Center, a DOE Office of

Science User Facility supported by the Office of Science of the U.S. Department of Energy under Contract No. DE-AC02-05CH11231.

- 
- [1] H. Kato, T. Okuda, Y. Okimoto, Y. Tomioka, K. Oikawa, T. Kamiyama, and Y. Tokura, *Phys. Rev. B* **69**, 184412 (2004), URL <http://link.aps.org/doi/10.1103/PhysRevB.69.184412>.
- [2] J. M. De Teresa, D. Serrate, C. Ritter, J. Blasco, M. R. Ibarra, L. Morellon, and W. Tokarz, *Phys. Rev. B* **71**, 092408 (2005), URL <http://link.aps.org/doi/10.1103/PhysRevB.71.092408>.
- [3] A. J. Hauser, J. R. Soliz, M. Dixit, R. E. A. Williams, M. A. Susner, B. Peters, L. M. Mier, T. L. Gustafson, M. D. Sumption, H. L. Fraser, et al., *Phys. Rev. B* **85**, 161201 (2012), URL <http://link.aps.org/doi/10.1103/PhysRevB.85.161201>.
- [4] D. Serrate, J. M. D. Teresa, and M. R. Ibarra, *Journal of Physics: Condensed Matter* **19**, 023201 (2007), URL <http://stacks.iop.org/0953-8984/19/i=2/a=023201>.
- [5] S. Vasala and M. Karppinen, *Progress in Solid State Chemistry* **43**, 1 (2015), ISSN 0079-6786, URL <http://www.sciencedirect.com/science/article/pii/S0079678614000338>.
- [6] M. P. Singh, K. D. Truong, S. Jandl, and P. Fournier, *Phys. Rev. B* **79**, 224421 (2009), URL <http://link.aps.org/doi/10.1103/PhysRevB.79.224421>.
- [7] J. B. Philipp, D. Reisinger, M. Schonecke, M. Opel, A. Marx, A. Erb, L. Alff, and R. Gross, *Journal of Applied Physics* **93**, 6853 (2003), URL <http://scitation.aip.org/content/aip/journal/jap/93/10/10.1063/1.1556124>.
- [8] K. I. Kobayashi, T. Kimura, H. Sawada, K. Terakura, and Y. Tokura, *Nature* **395**, 677 (1998), URL <http://dx.doi.org/10.1038/27167>.
- [9] N. Auth, G. Jakob, W. Westerburg, C. Ritter, I. Bonn, C. Felser, and W. Tremel, *Journal of Magnetism and Magnetic Materials* **272?276, Supplement**, E607 (2004), ISSN 0304-8853, proceedings of the International Conference on Magnetism (ICM 2003), URL <http://www.sciencedirect.com/science/article/pii/S0304885303021772>.
- [10] J. M. De Teresa, D. Serrate, J. Blasco, M. R. Ibarra, and L. Morellon, *Phys. Rev. B* **69**, 144401 (2004), URL <http://link.aps.org/doi/10.1103/PhysRevB.69.144401>.
- [11] H. Iwasawa, T. Saitoh, Y. Yamashita, D. Ishii, H. Kato, N. Hamada, Y. Tokura, and D. D. Sarma, *Phys. Rev. B* **71**, 075106 (2005), URL <http://link.aps.org/doi/10.1103/PhysRevB.71.075106>.
- [12] K. Oikawa, T. Kamiyama, H. Kato, and Y. Tokura, *Journal of the Physical Society of Japan* **72**, 1411 (2003), <http://dx.doi.org/10.1143/JPSJ.72.1411>, URL <http://dx.doi.org/10.1143/JPSJ.72.1411>.
- [13] B. Fisher, J. Genossar, K. Chashka, L. Patlagan, and G. Reisner, *Journal of Magnetism and Magnetic Materials* **316**, e713 (2007), ISSN 0304-8853, proceedings of the Joint European Magnetic Symposium, URL <http://www.sciencedirect.com/science/article/pii/S0304885307004076>.
- [14] E. Granado, Q. Huang, J. W. Lynn, J. Gopalakrishnan, R. L. Greene, and K. Ramesha, *Phys. Rev. B* **66**, 064409 (2002), URL <http://link.aps.org/doi/10.1103/PhysRevB.66.064409>.
- [15] W. Westerburg, O. Lang, C. Ritter, C. Felser, W. Tremel, and G. Jakob, *Solid State Communications* **122**, 201 (2002), ISSN 0038-1098, URL <http://www.sciencedirect.com/science/article/pii/S0038109802000790>.
- [16] H. Wu, *Phys. Rev. B* **64**, 125126 (2001), URL <http://link.aps.org/doi/10.1103/PhysRevB.64.125126>.
- [17] Z. Szotek, W. M. Temmerman, A. Svane, L. Petit, and H. Winter, *Phys. Rev. B* **68**, 104411 (2003), URL <http://link.aps.org/doi/10.1103/PhysRevB.68.104411>.
- [18] B. C. Jeon, C. H. Kim, S. J. Moon, W. S. Choi, H. Jeong, Y. S. Lee, J. Yu, C. J. Won, J. H. Jung, N. Hur, et al., *Journal of Physics: Condensed Matter* **22**, 345602 (2010), URL <http://stacks.iop.org/0953-8984/22/i=34/a=345602>.
- [19] V. N. Antonov, L. V. Bekenov, and A. Ernst, *Phys. Rev. B* **94**, 035122 (2016), URL <http://link.aps.org/doi/10.1103/PhysRevB.94.035122>.
- [20] A. Winkler, N. Narayanan, D. Mikhailova, K. G. Bramnik, H. Ehrenberg, H. Fuess, G. Vaitheeswaran, V. Kanchana, F. Wilhelm, A. Rogalev, et al., *New Journal of Physics* **11**, 073047 (2009), URL <http://stacks.iop.org/1367-2630/11/i=7/a=073047>.
- [21] H. Kato, T. Okuda, Y. Okimoto, Y. Tomioka, Y. Takenoya, A. Ohkubo, M. Kawasaki, and Y. Tokura, *Applied Physics Letters* **81**, 328 (2002), <http://dx.doi.org/10.1063/1.1493646>, URL <http://dx.doi.org/10.1063/1.1493646>.
- [22] H. Asano, N. Kozuka, A. Tsuzuki, and M. Matsui, *Applied Physics Letters* **85**, 263 (2004), URL <http://scitation.aip.org/content/aip/journal/apl/85/2/10.1063/1.1769085>.
- [23] A. J. Hauser, J. M. Lucy, H. L. Wang, J. R. Soliz, A. Holcomb, P. Morris, P. M. Woodward, and F. Y. Yang, *Applied Physics Letters* **102**, 032403 (2013), URL <http://scitation.aip.org/content/aip/journal/apl/102/3/10.1063/1.4789505>.
- [24] J. M. Lucy, A. J. Hauser, H. L. Wang, J. R. Soliz, M. Dixit, R. E. A. Williams, A. Holcombe, P. Morris, H. L. Fraser, D. W. McComb, et al., *Applied Physics Letters* **103**, 042414 (2013), URL <http://scitation.aip.org/content/aip/journal/apl/103/4/10.1063/1.4816803>.
- [25] P. Majewski, S. Geprgs, O. Sanganas, M. Opel, R. Gross, F. Wilhelm, A. Rogalev, and L. Alff, *Applied Physics Letters* **87**, 202503 (2005), URL <http://scitation.aip.org/content/aip/journal/apl/87/20/10.1063/1.2131178>.
- [26] J. M. Michalik, J. M. D. Teresa, C. Ritter, J. Blasco, D. Serrate, M. R. Ibarra, C. Kapusta, J. Freudenberger, and N. Kozlova, *EPL (Europhysics Letters)* **78**, 17006 (2007), URL <http://stacks.iop.org/0295-5075/78/i=1/a=17006>.

- [27] K. Kugel' and D. Khomskii, *Journal of Experimental and Theoretical Physics* **37**, 725 (1973), URL <http://www.jetp.ac.ru/cgi-bin/e/index/e/37/4/p725?a=list>.
- [28] Y. Tokura and N. Nagaosa, *Science* **288**, 462 (2000).
- [29] K. I. Kugel and D. I. Khomskii, *Soviet Physics Uspekhi* **25**, 231 (1982), URL <http://stacks.iop.org/0038-5670/25/i=4/a=R03>.
- [30] E. Pavarini, E. Koch, and A. I. Lichtenstein, *Phys. Rev. Lett.* **101**, 266405 (2008), URL <https://link.aps.org/doi/10.1103/PhysRevLett.101.266405>.
- [31] E. Pavarini, S. Biermann, A. Poteryaev, A. I. Lichtenstein, A. Georges, and O. K. Andersen, *Phys. Rev. Lett.* **92**, 176403 (2004), URL <https://link.aps.org/doi/10.1103/PhysRevLett.92.176403>.
- [32] E. Pavarini, A. Yamasaki, J. Nuss, and O. K. Andersen, *New Journal of Physics* **7**, 188 (2005), URL <http://stacks.iop.org/1367-2630/7/i=1/a=188>.
- [33] W.-G. Yin, D. Volja, and W. Ku, *Phys. Rev. Lett.* **96**, 116405 (2006), URL <https://link.aps.org/doi/10.1103/PhysRevLett.96.116405>.
- [34] A. I. Liechtenstein, V. I. Anisimov, and J. Zaanen, *Phys. Rev. B* **52**, R5467 (1995), URL <http://link.aps.org/doi/10.1103/PhysRevB.52.R5467>.
- [35] I. Leonov, N. Binggeli, D. Korotin, V. I. Anisimov, N. Stojić, and D. Vollhardt, *Phys. Rev. Lett.* **101**, 096405 (2008), URL <https://link.aps.org/doi/10.1103/PhysRevLett.101.096405>.
- [36] L. J. P. Ament and G. Khaliullin, *Phys. Rev. B* **81**, 125118 (2010), URL <https://link.aps.org/doi/10.1103/PhysRevB.81.125118>.
- [37] M. Mochizuki and M. Imada, *Journal of the Physical Society of Japan* **73**, 1833 (2004), <http://dx.doi.org/10.1143/JPSJ.73.1833>, URL <http://dx.doi.org/10.1143/JPSJ.73.1833>.
- [38] M. Mochizuki and M. Imada, *New Journal of Physics* **6**, 154 (2004), URL <http://stacks.iop.org/1367-2630/6/i=1/a=154>.
- [39] J. Akimitsu, H. Ichikawa, N. Eguchi, T. Miyano, M. Nishi, and K. Kakurai, *Journal of the Physical Society of Japan* **70**, 3475 (2001), <http://dx.doi.org/10.1143/JPSJ.70.3475>, URL <http://dx.doi.org/10.1143/JPSJ.70.3475>.
- [40] M. Itoh, M. Tsuchiya, H. Tanaka, and K. Motoya, *Journal of the Physical Society of Japan* **68**, 2783 (1999), <http://dx.doi.org/10.1143/JPSJ.68.2783>, URL <http://dx.doi.org/10.1143/JPSJ.68.2783>.
- [41] T. Kiyama, H. Saitoh, M. Itoh, K. Kodama, H. Ichikawa, and J. Akimitsu, *Journal of the Physical Society of Japan* **74**, 1123 (2005), <http://dx.doi.org/10.1143/JPSJ.74.1123>, URL <http://dx.doi.org/10.1143/JPSJ.74.1123>.
- [42] F. Iga, M. Tsubota, M. Sawada, H. B. Huang, S. Kura, M. Takemura, K. Yaji, M. Nagira, A. Kimura, T. Jo, et al., *Phys. Rev. Lett.* **93**, 257207 (2004), URL <https://link.aps.org/doi/10.1103/PhysRevLett.93.257207>.
- [43] H. Nakao, Y. Wakabayashi, T. Kiyama, Y. Murakami, M. v. Zimmermann, J. P. Hill, D. Gibbs, S. Ishihara, Y. Taguchi, and Y. Tokura, *Phys. Rev. B* **66**, 184419 (2002), URL <https://link.aps.org/doi/10.1103/PhysRevB.66.184419>.
- [44] B. Keimer, D. Casa, A. Ivanov, J. W. Lynn, M. v. Zimmermann, J. P. Hill, D. Gibbs, Y. Taguchi, and Y. Tokura, *Phys. Rev. Lett.* **85**, 3946 (2000), URL <https://link.aps.org/doi/10.1103/PhysRevLett.85.3946>.
- [45] J.-G. Cheng, Y. Sui, J.-S. Zhou, J. B. Goodenough, and W. H. Su, *Phys. Rev. Lett.* **101**, 087205 (2008), URL <https://link.aps.org/doi/10.1103/PhysRevLett.101.087205>.
- [46] M. Cwik, T. Lorenz, J. Baier, R. Müller, G. André, F. Bourée, F. Lichtenberg, A. Freimuth, R. Schmitz, E. Müller-Hartmann, et al., *Phys. Rev. B* **68**, 060401 (2003), URL <https://link.aps.org/doi/10.1103/PhysRevB.68.060401>.
- [47] J. Hemberger, H.-A. K. von Nidda, V. Fritsch, J. Deisenhofer, S. Lobina, T. Rudolf, P. Lunkenheimer, F. Lichtenberg, A. Loidl, D. Bruns, et al., *Phys. Rev. Lett.* **91**, 066403 (2003), URL <https://link.aps.org/doi/10.1103/PhysRevLett.91.066403>.
- [48] M. N. Iliev, A. P. Litvinchuk, M. V. Abrashev, V. N. Popov, J. Cmaidalka, B. Lorenz, and R. L. Meng, *Phys. Rev. B* **69**, 172301 (2004), URL <https://link.aps.org/doi/10.1103/PhysRevB.69.172301>.
- [49] V. Fritsch, J. Hemberger, M. V. Eremin, H.-A. Krug von Nidda, F. Lichtenberg, R. Wehn, and A. Loidl, *Phys. Rev. B* **65**, 212405 (2002), URL <https://link.aps.org/doi/10.1103/PhysRevB.65.212405>.
- [50] T. Arima, Y. Tokura, and J. B. Torrance, *Phys. Rev. B* **48**, 17006 (1993), URL <https://link.aps.org/doi/10.1103/PhysRevB.48.17006>.
- [51] Y. Taguchi, Y. Tokura, T. Arima, and F. Inaba, *Phys. Rev. B* **48**, 511 (1993), URL <https://link.aps.org/doi/10.1103/PhysRevB.48.511>.
- [52] Y. Okimoto, T. Katsufuji, Y. Okada, T. Arima, and Y. Tokura, *Phys. Rev. B* **51**, 9581 (1995), URL <https://link.aps.org/doi/10.1103/PhysRevB.51.9581>.
- [53] M. T. HUTCHINGS, E. J. SAMUELSEN, G. SHIRANE, and K. HIRAKAWA, *Phys. Rev.* **188**, 919 (1969), URL <https://link.aps.org/doi/10.1103/PhysRev.188.919>.
- [54] L. Paolasini, R. Caciuffo, A. Sollier, P. Ghigna, and M. Altarelli, *Phys. Rev. Lett.* **88**, 106403 (2002), URL <https://link.aps.org/doi/10.1103/PhysRevLett.88.106403>.
- [55] L. G. Marshall, J. Zhou, J. Zhang, J. Han, S. C. Vogel, X. Yu, Y. Zhao, M. T. Fernández-Díaz, J. Cheng, and J. B. Goodenough, *Phys. Rev. B* **87**, 014109 (2013), URL <https://link.aps.org/doi/10.1103/PhysRevB.87.014109>.
- [56] F. Moussa, M. Hennion, J. Rodríguez-Carvajal, H. Moudou, L. Pinsard, and A. Revcolevschi, *Phys. Rev. B* **54**, 15149 (1996), URL <https://link.aps.org/doi/10.1103/PhysRevB.54.15149>.
- [57] M. C. Sánchez, G. Subías, J. García, and J. Blasco, *Phys. Rev. Lett.* **90**, 045503 (2003), URL <https://link.aps.org/doi/10.1103/PhysRevLett.90.045503>.
- [58] G. Chen, R. Pereira, and L. Balents, *Phys. Rev. B* **82**, 174440 (2010), URL <https://link.aps.org/doi/10.1103/PhysRevB.82.174440>.
- [59] A. S. Erickson, S. Misra, G. J. Miller, R. R. Gupta, Z. Schlesinger, W. A. Harrison, J. M. Kim, and I. R. Fisher, *Phys. Rev. Lett.* **99**, 016404 (2007), URL <https://link.aps.org/doi/10.1103/PhysRevLett.99.016404>.
- [60] K. E. Stitzer, M. D. Smith, and H.-C. zur Loye, *Solid State Sciences* **4**, 311 (2002), ISSN 1293-2558, URL <http://www.sciencedirect.com/science/article/pii/S1293255801012572>.

- [61] A. J. Steele, P. J. Baker, T. Lancaster, F. L. Pratt, I. Franke, S. Ghannadzadeh, P. A. Goddard, W. Hayes, D. Prabhakaran, and S. J. Blundell, *Phys. Rev. B* **84**, 144416 (2011), URL <https://link.aps.org/doi/10.1103/PhysRevB.84.144416>.
- [62] H. J. Xiang and M.-H. Whangbo, *Phys. Rev. B* **75**, 052407 (2007), URL <https://link.aps.org/doi/10.1103/PhysRevB.75.052407>.
- [63] J. Romhányi, L. Balents, and G. Jackeli, *Phys. Rev. Lett.* **118**, 217202 (2017), URL <https://link.aps.org/doi/10.1103/PhysRevLett.118.217202>.
- [64] K.-W. Lee and W. E. Pickett, *EPL (Europhysics Letters)* **80**, 37008 (2007), URL <http://stacks.iop.org/0295-5075/80/i=3/a=37008>.
- [65] S. Gangopadhyay and W. E. Pickett, *Phys. Rev. B* **93**, 155126 (2016), URL <https://link.aps.org/doi/10.1103/PhysRevB.93.155126>.
- [66] S. Gangopadhyay and W. E. Pickett, *Phys. Rev. B* **91**, 045133 (2015), URL <https://link.aps.org/doi/10.1103/PhysRevB.91.045133>.
- [67] S. Kanungo, K. Mogare, B. Yan, M. Reehuis, A. Hoser, C. Felser, and M. Jansen, *Phys. Rev. B* **93**, 245148 (2016), URL <http://link.aps.org/doi/10.1103/PhysRevB.93.245148>.
- [68] P. E. Blöchl, *Phys. Rev. B* **50**, 17953 (1994), URL <http://link.aps.org/doi/10.1103/PhysRevB.50.17953>.
- [69] G. Kresse and D. Joubert, *Phys. Rev. B* **59**, 1758 (1999).
- [70] G. Kresse and D. Joubert, *Phys. Rev. B* **59**, 1758 (1999), URL <http://link.aps.org/doi/10.1103/PhysRevB.59.1758>.
- [71] J. P. Perdew, A. Ruzsinszky, G. I. Csonka, O. A. Vydrov, G. E. Scuseria, L. A. Constantin, X. Zhou, and K. Burke, *Phys. Rev. Lett.* **100**, 136406 (2008), URL <http://link.aps.org/doi/10.1103/PhysRevLett.100.136406>.
- [72] H. Park, A. J. Millis, and C. A. Marianetti, *Phys. Rev. B* **92**, 035146 (2015), URL <http://link.aps.org/doi/10.1103/PhysRevB.92.035146>.
- [73] J. Chen, A. J. Millis, and C. A. Marianetti, *Phys. Rev. B* **91**, 241111 (2015), URL <http://link.aps.org/doi/10.1103/PhysRevB.91.241111>.
- [74] C. A. Marianetti, D. Morgan, and G. Ceder, *Phys. Rev. B* **63**, 224304 (2001).
- [75] B. H. Kim, G. Khaliullin, and B. I. Min, *Phys. Rev. Lett.* **109**, 167205 (2012), URL <https://link.aps.org/doi/10.1103/PhysRevLett.109.167205>.
- [76] H. Watanabe, T. Shirakawa, and S. Yunoki, *Phys. Rev. Lett.* **105**, 216410 (2010), URL <https://link.aps.org/doi/10.1103/PhysRevLett.105.216410>.
- [77] B. J. Kim, H. Jin, S. J. Moon, J.-Y. Kim, B.-G. Park, C. S. Leem, J. Yu, T. W. Noh, C. Kim, S.-J. Oh, et al., *Phys. Rev. Lett.* **101**, 076402 (2008), URL <https://link.aps.org/doi/10.1103/PhysRevLett.101.076402>.
- [78] S. Nakamura and K. Oikawa, *Journal of the Physical Society of Japan* **72**, 3123 (2003), <http://dx.doi.org/10.1143/JPSJ.72.3123>, URL <http://dx.doi.org/10.1143/JPSJ.72.3123>.
- [79] J. M. Lucy, M. R. Ball, O. D. Restrepo, A. J. Hauser, J. R. Soliz, J. W. Freeland, P. M. Woodward, W. Windl, and F. Y. Yang, *Phys. Rev. B* **90**, 180401 (2014), URL <http://link.aps.org/doi/10.1103/PhysRevB.90.180401>.
- [80] J. M. Lucy, A. J. Hauser, Y. Liu, H. Zhou, Y. Choi, D. Haskel, S. G. E. te Velthuis, and F. Y. Yang, *Phys. Rev. B* **91**, 094413 (2015), URL <https://link.aps.org/doi/10.1103/PhysRevB.91.094413>.
- [81] S. Gong, S.-D. Guo, P. Chen, and B.-G. Liu, *RSC Adv.* **5**, 63165 (2015), URL <http://dx.doi.org/10.1039/C5RA09921H>.
- [82] E. B. Isaacs and C. A. Marianetti, *Phys. Rev. B* **95**, 045141 (2017).
- [83] M. Sikora, C. Kapusta, M. Borowiec, C. J. Oates, V. Prochazka, D. Rybicki, D. Zajac, J. M. De Teresa, C. Marquina, and M. R. Ibarra, *Applied Physics Letters* **89**, 062509 (2006), URL <http://scitation.aip.org/content/aip/journal/apl/89/6/10.1063/1.2234292>.
- [84] D. Serrate, J. M. D. Teresa, P. A. Algarabel, C. Marquina, J. Blasco, M. R. Ibarra, and J. Galibert, *Journal of Physics: Condensed Matter* **19**, 436226 (2007), URL <http://stacks.iop.org/0953-8984/19/i=43/a=436226>.
- [85] H.-T. Jeng and G. Y. Guo, *Phys. Rev. B* **67**, 094438 (2003), URL <http://link.aps.org/doi/10.1103/PhysRevB.67.094438>.
- [86] G. Vaitheeswaran, V. Kanchana, and A. Delin, *Applied Physics Letters* **86**, 032513 (2005), URL <http://scitation.aip.org/content/aip/journal/apl/86/3/10.1063/1.1855418>.
- [87] S.-D. Guo, *The European Physical Journal B* **88**, 82 (2015), ISSN 1434-6036, URL <http://dx.doi.org/10.1140/epjb/e2015-50883-1>.
- [88] G. Kotliar, S. Y. Savrasov, K. Haule, V. S. Oudovenko, O. Parcollet, and C. A. Marianetti, *Rev. Mod. Phys.* **78**, 865 (2006).
- [89] A. C. Komarek, S. V. Streltsov, M. Isobe, T. Möller, M. Hoelzel, A. Senyshyn, D. Trots, M. T. Fernández-Díaz, T. Hansen, H. Gotou, et al., *Phys. Rev. Lett.* **101**, 167204 (2008), URL <http://link.aps.org/doi/10.1103/PhysRevLett.101.167204>.
- [90] M. Cococcioni and S. de Gironcoli, *Phys. Rev. B* **71**, 035105 (2005), URL <http://link.aps.org/doi/10.1103/PhysRevB.71.035105>.